Journal of Applied Physics PERSPECTIVE scitation.org/journal/jap

Short-wave IR ultrafast fiber laser systems: Current challenges and prospective applications

Cite as: J. Appl. Phys. **128**, 180906 (2020); doi: 10.1063/5.0023936
Submitted: 5 August 2020 · Accepted: 25 October 2020 ·
Published Online: 12 November 2020

D. C. Kirsch,[1] S. Chen,[2] R. Sidharthan,[2] Y. Chen,[2] S. Yoo,[2] and M. Chernysheva[1,a)]

AFFILIATIONS

[1]Leibniz Institute of Photonic Technology, Albert-Einstein St. 9, 07745 Jena, Germany
[2]School of Electrical and Electronic Engineering, Nanyang Technological University, 50 Nanyang Ave., Singapore 639798

[a)]**Author to whom correspondence should be addressed:** Maria.Chernysheva@leibniz-ipht.de

ABSTRACT

Ultrashort pulse generation at the short-wave infrared (SWIR) wavelength ranges from 1.6 to 2.5 μm and together with benefits of the all-fiber design has transformed lasers into an essential tool for industrial, technological, scientific, environmental, and medical applications. With the development of pumping sources and fiber components, ultrafast SWIR fiber lasers have drawn exceptional research and industrial attention over the last decade, resulting in the achievement of comparable performance or even surpassing well-established near-IR sources. Exceptionally compact, highly stable, cost-effective, and maintenance-free ultrafast fiber lasers operating at the SWIR range are currently well on the way to be commercially employed. This invited Perspective article gives a comprehensive overview of the most significant achievements enabling ultrafast generation at SWIR, including up-to-date gain fibers and saturable absorbers, nonlinear process, and laser architectures. This article highlights the perspectives and strategies for further maturing of the field of SWIR fiber lasers and pathways for the improvement of the performance, overcoming existing bottlenecks and challenges toward reducing pulse durations, tunability of repetition rate, and power upscaling. The advancement of the ultrafast SWIR laser development is projected until the landscape of existing technologies, driven by these ultimate sources, and potential applications, emerging on the horizon.

I. INTRODUCTION

Lasers have inspired numerous research fields and technologies and have been placed at the frontier of interdisciplinary research and development as a critical enabling technological platform. Laser systems are developed on a very different scale and temporal, spectral, and intensity performance levels, tailored to match requirements set by the specific application. Thus, numerous hidden high-speed and high-intensity phenomena in physics, chemistry, or biology,[1–4] such as the real-time observation of molecular motion in chemical reactions[5,6] or measurement of fundamental constants with ultraprecise uncertainties,[7,8] have been exposed by the application of lasers with the ultrashort pulsed operation, as predicted by DiDominico[9] and demonstrated for the first time by Hargrove *et al.*[10] in 1964. The term ultrashort is referred to sub-picosecond to few femtosecond pulse duration or even single-cycle operation. The generation of such pulses is, generally, achieved by managing intensity-selective losses in the laser cavity, while multiple longitudinal resonator modes interfere coherently and constructively to circumvent these losses. This process leads to well-defined wave packets with just several oscillation periods but with exceptionally high pulse peak powers at the same average power of a continuous wave. This principle is realized in the so-called mode-locking technique, which currently is the most commonly used.[11] Although gain-[12] or Q-switching[13] is capable of reaching hundreds of picoseconds duration in the most extreme cases, such pulses are conventionally not considered as ultrashort. For plenty of conventional material processing, metrology, or imaging tenders, ultrafast lasers have shown higher accuracy, faster data acquisition, or lower processing time due to their higher pulse peak powers, repetition rates, and lower levels of noise, when compared to continuous-wave systems.

Maturing ultrafast laser systems have offered robust, compact, turn-key operable, and cost-effective solutions to explore their potential in the industrial sector in full. While conventional solid-state lasers require vibration-less operation conditions with stabilized temperature and humidity, the monolithic all-fiber laser configuration offers an elegant solution with excellent performance for ultrashort pulse generation. Fiber lasers offer the desirable compromise between the output power and the instrument footprint

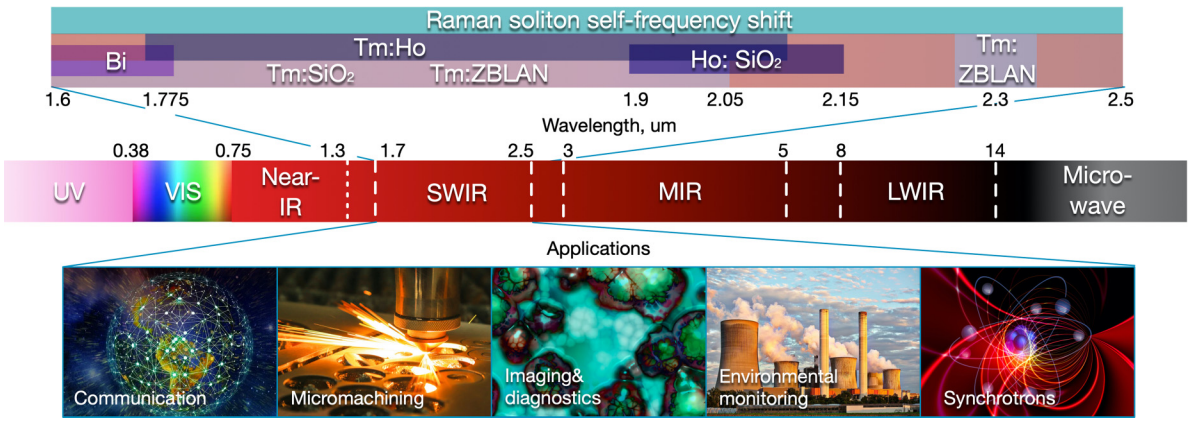

FIG. 1. SWIR wavelength, available gain media, and prospective applications.

and superior beam quality toward high output, when compared to alternative techniques, including thin-disk, microchip, and semiconductor lasers.[14,15]

When we think of commercially available ultrafast light sources, well-established titanium:sapphire or ytterbium-doped fiber-based technologies[16] operating in the near-infrared wavelength region, around 1 μm, come to one's mind, which have proved their efficiency in diverse applications. Nonetheless, newly emerging applications, together with significant enhancement of existing ones, can be achieved by shifting ultrashort pulse generation toward longer operational wavelengths, such as the short-wavelength infrared (SWIR) range. The modern literature shows quite a wide variety of spectral band definitions for SWIR wavelengths, ranging from 1 to 3 μm. In the current review, we will discuss a range between 1.6 and 2.5 μm (Fig. 1). While it falls within the silica glass transparency window from 0.2 to 2.5 μm, the SWIR range features distinct characteristics. From the atmospheric window of high transparency beyond 2 μm for eye-safe, long-distance, free-space assignments,[17] over various molecules' absorption lines for spectroscopy,[18,19] medicine,[20] or micro-machining,[21] to the utmost penetration depth in the biological tissue at around 1.7 μm for imaging,[22,23] there are a plethora of wonderful features that we will discuss in the current Perspective. Even though the operational wavelength range of erbium-doped silica fibers operates from 1.5 to 1.6 μm falls in some of SWIR definitions, we will not cover it in the current Perspective. The features and challenges of this wavelength range, typically referred to as telecommunication band, differ significantly from the specified SWIR range and, thus, go beyond the scope of this Perspective.

Back in the beginning of 2010s, the market of fiber-optic components was generally limited, supplying mainly optical telecommunications for 1310–1555 nm wavelength range. Driven by application demand, the last decade demonstrated an expanded market of silica fiber components and nowadays, almost covering the entire range from 0.7 to 2.1 μm. Within the same time, individual SWIR ultrafast lasers have matured out, and the first systems have now become commercially available. We want to take this phenomenal advancement to evaluate the current state of the art on such lasers and highlight their performance capabilities together with application requirements, paying particular attention to usability. Discussing the whole process of ultrafast SWIR fiber lasers, we provide insight into the current trends, challenges, and perspectives of several research areas, including material science, fiber optics, laser physics, and nonlinear optics. In this Perspective, we aim to provide a comprehensive overview of exciting possibilities of ultrashort pulse generation at SWIR wavelength and indicate a vector for future research and development.

The outline of the current Perspective is the following: in Sec. II, we will portray active ions for SWIR thulium and holmium, as well as Raman-gain, followed by different options to initiate mode-locking, shape, and stabilize pulses. Section III provides an overview of ultrafast thulium-doped fiber lasers, as the most developed systems at SWIR. We will review different operational regimes, mostly due to management of intracavity dispersion. In Sec. IV, we will discuss laser applications and will elaborate on competing solutions and their benefits for remarkable novel purposes. Finally, in Sec. V, we will discuss whether novel host materials and fiber geometries could surmount today's restraints in power scaling self-starting all-fiber systems.

II. LASER MATERIALS ENABLING ULTRAFAST GENERATION AT SWIR

A. Active optical fibers

In the spectral range of the SWIR, Tm^{3+}, Ho^{3+}, Bi^{x+}, Er^{3+}, Pr^{3+}, Nd^{3+}, Cr^{2+}, Co^{2+}, Ni^{2+}, U^{3+}, and Dy^{2+} are potential laser-active ions. Among these, in turn, just Tm-, Ho-, Tm/Ho-, and Bi-doped fibers have demonstrated the effective generation of ultrashort pulses and are subject to comprehensive research nowadays (Fig. 1). The remaining materials show significant obstacles in achieving high efficiency, mainly due to strict temperature requirements or limited pump sources accessibility. Where the required wavelength is not accessible by direct generation from active ions, various nonlinear approaches can be utilized, such as Raman

frequency conversion or soliton self-frequency shift. Wavelength conversion is realized by the application of highly nonlinear fibers, preserving the medium dispersion anomalous, particularly, for the soliton self-frequency shift. The bright demonstrated examples of nonlinear media are microstructured tellurite, fluoride, highly doped germanium, and active thulium-doped fibers. The application of such media has enabled the generation of high-quality Raman solitons with ~100 fs duration tunable from 2 to 2.65 μm, thus reaching the longer edge of the SWIR range[24–27] (Fig. 1).

1. Thulium-doped fibers

Tm-doped fibers (TDFs) have been the primary gain medium for lasers working in 1.7−2.05 μm region due to the broad emission spectrum of Tm^{3+} ions spanning almost the entire SWIR range. Tm^{3+} has been asserted latterly as the second most efficient laser-active ion after Yb^{3+}.

The four lowest manifolds ($^3H_6$, $^3F_4$, $^3H_5$, and $^3H_4$ levels) of the Tm^{3+} ion provide efficient energy transition paths[29] as shown in Fig. 2(a). The major pumping routes used in ultrafast lasers and the cross-relaxation mechanism ($^3H_6$, $^3H_4 \rightarrow {}^3F_4$, $^3F_4$) are presented in the diagram. The Tm^{3+} ion can be pumped to the $^3F_4$ manifold by multiple wavebands centered around 0.46, 0.67, 0.79, 1.21, and 1.6 μm. Among the various pumping schemes, the 0.79 μm and the 1.6 μm pumping routes [I and II, respectively, in Fig. 2(a)] are the most popular in mode-locked TDF lasers as well as continuous wave lasers.[30–33] The 1.6 μm pump scheme involves direct pumping to the emission band at 1.9 μm, using high brightness lasers such as an Er-doped fiber laser. It offers an in-band pumping scheme with high efficiency. On the other hand, the pump scheme at 0.79 μm enjoys the availability of high-power laser diodes. Still, it has limited efficiency due to the Stokes limit of only about 40%. Fortunately, with sufficient Tm^{3+} ion concentration, operation efficiency is vastly increased (a theoretical maximum of 80%) by realizing the so-called "two-for-one" cross-relaxation depicted in Fig. 2(a). Pumped by one 0.79 μm photon, one Tm^{3+} ion at ground state of $^3H_6$ gets excited to $^3H_4$ level (I). Then, this ion at $^3H_4$ rests to the $^3F_4$ (IV) level, which subsequently energizes another Tm^{3+} ion to the $^3F_4$ level from the ground state level, $^3H_6$ (V). Thus, two laser photons are generated with emission routes III and VI by one photon pumped to the $^3H_4$ level. The high Tm concentration is vital to realize the cross-relaxation process, yet it increases the possibility of clustering.

However, the required high concentration brings along undesired non-radiative energy transfer, such as excited state absorption (ESA) and energy transfer upconversion (ETU). The ESA occurs due to pump absorption by excited Tm^{3+} ions causing them to get excited to even higher energy levels (based on near-resonant energy transition with the pump), adversely affecting lasing efficiency. The ESA happens at both the 0.79 and 1.6 μm pumping schemes, albeit not significant, following the transition $^3H_5$ or $^3H_4 \rightarrow {}^1G_4$ and $^3F_4 \rightarrow {}^3H_4$, respectively,[33,34] depicted by dashed violet arrows in Fig. 2(a). In its turn, the ETU occurs between a pair of excited Tm^{3+} ions, where one of the ions is raised to higher energy level while the other is demoted to a lower energy level. ETU transitions are depicted by dashed green arrows in Fig. 2(a). ETU processes have a non-negligible effect on lifetime quenching of $^3F_4$ multiplet, with the transition $^3F_4$, $^3F_4 \rightarrow {}^3H_4$, $^3H_6$ having a significantly larger impact particularly with larger clustering.[35,36] The ETU via the transitions $^3H_4 \rightarrow {}^3F_4$, $^1G_4$ is manifested by blue fluorescence under 0.79 μm pumping.

1. Limits of silica fibers and alternatives. So far, our discussion in the Tm-doped fiber laser (TDFL) covered only silica-based glass matrix. Silica glass offers advantages of low nonlinearity, high physical strength, chemical durability, high softening temperature, and low thermal expansion coefficient that help it withstand high powers. Silica glass matrix should be carefully designed to increase the rare-earth ion concentration and reduce quenching or clustering issues. Thus, in the case of multi-component Tm-doped silica

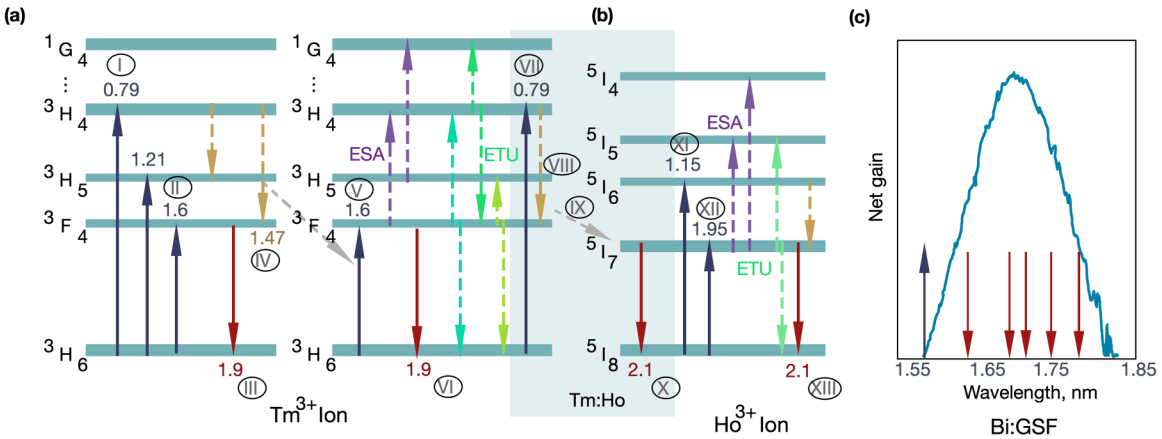

FIG. 2. Simplified energy diagrams of (a) Tm, (b) Ho-doped silica. Highlighted area represents transitions for Tm:Ho co-doping. The solid arrows represent a radiative transition, and the dashed arrows indicate a non-radiative transition. ETU: energy transfer upconversion (dashed green arrows), ESA: excited state absorption (dashed violet arrows). (c) Schematic optical gain spectrum of Bi-GSF. Adapted with permission from Firstov *et al.*, Opt. Lett. **39**, 6927–6930 (2014). Copyright 2014 The Optical Society.

fibers, aluminium (Al) presents an effective co-dopant that enhances the solubility of Tm ions in a silica glass matrix and reduces undesirable energy transfers. Addition of phosphorous (P) is also known to improve Tm ions solubility. However, the use of P as a co-dopant in Tm fibers is rare because it increases the phonon energy and could facilitate non-radiative transitions, such as $^3H_4 \rightarrow ^3 H_5$ and, therefore, reduces the efficiency of the cross-relaxation process.[37] Despite the Tm emission down to 1.6 μm, the achievement of laser generation below 1.8 μm is generally challenging due to strong re-absorption. Nevertheless, Tm spectroscopic properties can be adjusted in favor of the shorter wavelength emission. In particular, co-doping with germanium (Ge) is found useful to blue shift the Tm absorption and emission cross sections.[38,39] We will discuss this in more detail in Sec. III B.

On the other hand, large dispersion and higher loss at longer wavelengths (>2 μm) of silica pose challenges in controlling cavity dispersion and reaching longer wavelengths. Moreover, high phonon energy and low rare-earth solubility of silica set the limit for the laser quantum efficiency.[35–37] In this end, very high Tm concentration was reported in a germanosilicate (GSF) glass, which allowed cladding-pumped mode-locked laser.[40]

2. ZBLAN. The most successful non-silica fiber in the study of mode-locked lasers would be fluoride fibers, particularly, $ZrF_4-BaF_2-LaF_3-AlF_3$–NaF (ZBLAN) fiber. They offer a broad transmission window, low phonon energy, smaller dispersion values, and a low refractive index.[41,42] Thus, a Tm-doped ZBLAN fiber was reported to generate 45 fs pulse with ~37 nJ without the help of a compression stage.[43] Unfortunately, the lack of fiber components made of fluoride glasses and complicated fiber fabrication and post-processing restrict the development of an all-fiber laser system. All-fiberized ZBLAN-based fiber laser is currently not available due to significantly different softening temperatures and other material properties between silica-based fiber components and ZBLAN fibers.

2. Holmium-doped fibers

For wavelengths above 2.05 μm, power and pulse energy decrease considerably for TDFLs due to the reduced emission cross section. In this regard, Ho-doped fibers (HDFs) can be considered for the laser wavelength of 2−2.15 μm in silica fiber. The simplified energy level diagram for a Ho-doped silica fiber is shown in Fig. 2(b).[44] Two major pumping routes are $^5I_8 \rightarrow ^5 I_6$ (XI) and $^5I_8 \rightarrow ^5 I_7$ (XII) corresponding to ~1.15 μm and 1.95 μm wavelengths, respectively, both of which could excite Ho^{3+} ions from the ground state to the $^5I_7$ level for lasing.[45–48] In case of the 1.15 μm pumping (XI), the $^5I_6$ level can be accessed by laser diodes, ytterbium-doped fiber lasers (YDFLs) or Raman lasers.[45,46] Nonetheless, direct resonant pumping at 1.95 μm (XII) offered by efficient high-power TDFL is the main pumping scheme for efficient high-power Ho-doped fiber lasers (HDFLs).[47,48] Similar to TDFL, the quenching mechanisms substantially hinder the efficiency of HDFL. When the 1.15 μm pump ($^5I_8 \rightarrow ^5 I_6$) is used, an ESA can occur via the transition $^5I_7 \rightarrow ^5 I_4$ as shown in Fig. 2(b).[49] Similarly, with the 1.95 μm pump ($^5I_8 \rightarrow ^5 I_7$), an ESA can occur following the transition $^5I_7 \rightarrow ^5 I_5$. An ETU, on the other hand, is activated following $^5I_7 \rightarrow ^5 I_8$ and $^5I_7 \rightarrow ^5 I_5$ under the 1.95 μm pump scheme. Also, background loss and OH absorption coupled with the limited concentration set by the ESA become main barrier for efficient HDFL operating at the wavelength >2.1 μm.

Mode-locking in Ho-doped silica fibers typically has output wavelengths in the range of 1.9−2.13 μm. Compared to the Tm counterpart, progress in mode-locked HDFLs has been relatively slow. Femtosecond pulses were demonstrated for 160 fs laser (98 fs after compression) with the energy of 1 nJ at 2060 nm[50] and 212 fs with 3.79 nJ at 2079 nm.[51]

3. Tm:Ho co-doped fibers

Co-doping by Tm^{3+} and Ho^{3+} can diversify pumping schemes. In Tm:Ho fibers, pumping schemes at 0.79 or 1.55 μm can be employed to excite Tm^{3+} ions from ground state $^3H_6$ to the metastable level $^3F_4$ (transition V in Fig. 2). In case of pumping at 0.79 μm (transition VII), Tm^{3+} undergoes non-radiative relaxation from $^3H_4$ to $^3F_4$ (transition VIII). Subsequently, Ho^{+3} ion is getting excited to level $^5I_7$ via the resonant energy transfer from Tm^{3+} ion at $^3F_4$ level (transition IX). The laser generation is achieved with the transition of Ho^{3+} from $^5I_7$ level to the ground state (transition X in Fig. 2).[52–55] Mode-locking in a Tm:Ho fiber under 0.79 μm core pumping was demonstrated to generate 315 fs pulse with ~1 nJ at 1968 nm.[56]

4. Bismuth-doped fibers

Intensive research has demonstrated alternative active media, not based on conventional rare-earth elements, but such as bismuth (Bi). Since the early 2000s, numerous types of Bi-doped optical fibers have been investigated and used for the development of Bi-doped fiber lasers and optical amplifiers.[57–59] Interestingly, bismuth enables emission only in fibers, while a bulk Bi-doped glass has not yet demonstrated laser generation. Bismuth remains mysterious polyvalent element since its luminescence nature has not been related to individual oxidation states (Bi^{5+}, Bi^{3+}, Bi^{2+}, and Bi^{+}) or associated glass matrix composition, so far.

Bi-doped optical fibers exhibit broadband luminescence spanning from 1000 to 2000 nm. The emission of Bi centers can be extended to SWIR wavelength ranges from 1.6 to 1.8 μm [Fig. 2(c)] by the fabrication of silica fibers with high GeO_2 concentration (above 50%).[28] Being at the very beginning of their investigation, ultrashort pulse Bi-doped fiber lasers operating at 1650–1750 nm have proved their potential for application in multiphoton microscopy and showing the performance comparable with laser systems based on the Raman soliton shift. One of the drawbacks of Bi-doped active media is the limited concentration of active Bi-ions and, therefore, low amplification. Thus, extended lengths of the active fiber are required to achieve higher laser generation efficiency at the expense limited fundamental repetition rate of ultrashort pulse generation at several MHz.[60] In contrast, higher frequencies up to 200 MHz can be achieved only by harmonic mode-locking.[61] On the other hand, the required high content of GeO_2 in the Bi-doped fiber shifts the zero-dispersion wavelength to the SWIR region, providing lots of space for ultrashort pulse peak power upscaling by managing net-cavity dispersion.[61] The characteristics were utilized to develop an ultrafast laser with 17 ps (compressed to

630 fs) pulses at 1.7 μm with a pulse energy of 5.7 nJ.[60] Further energy upscaling seems to depend on material optimization toward increasing the gain and lowering the losses.

5. Prospects on fiber development

1. New geometries for dispersion control. To date, the anomalous dispersion of silica-based fibers beyond 1.7 μm dominantly restricts the performance of SWIR ultrafast fiber lasers in regard to net-cavity dispersion management. One of the possible approaches to achieve normal dispersion in silica-based fibers is decreasing fiber core diameter down to ~2 μm[43,62] together with increasing the concentration of germanium oxide.[31,63–65] However, very high nonlinearity in such small core fiber introduces limitations on the pulse energy. Alternatively, ZBLAN fibers can exhibit normal dispersion at the SWIR range due to their smaller negative material dispersion than silica glass fiber.[41,42] However, using ZBLAN fibers for all-fiber laser systems appears too difficult due to the lack of ZBLAN-based fiber components. Therefore, silica-based normal dispersion fibers would present an optimal platform, at least for the time being, for a monolithic system.

It is well known that modeling the refractive index profile of silica fibers by suppressing the cladding (or segmented-core) refractive index allows compensation of the material dispersion by the waveguide dispersion.[67,68] Thus, the so-called W-type index profile (see the left inset in Fig. 3) can shift zero-dispersion wavelength in silica fibers toward ~2 μm. In Refs. 39 and 66, the authors demonstrated a W-type normal dispersion TDF with a core size of 5 μm, exhibiting a normal dispersion in the broad wavelength range spanning 1.6−2.1 μm region. Figure 3 shows the dispersion spectrum of the fiber with maximum normal dispersion of −11.3 ps/nm km at 1.85−1.95 μm. The W-type normal dispersion TDF could be further improved in an aspect of glass composition with higher Tm doping concentration (to achieve higher gain), and in a waveguide design for larger normal dispersion value in the SWIR region. It is worth mentioning that a W-type normal dispersion TDF also

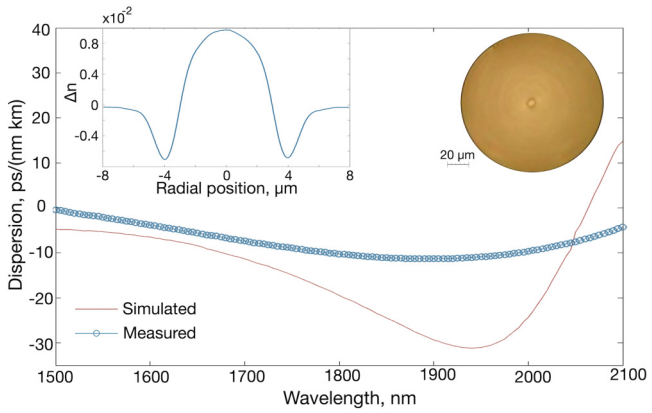

FIG. 3. Example of dispersion curves of W-type thulium-doped fiber in the SWIR region. Inset: fiber's refractive index profile and its cross section. Adapted from Chen *et al.*, IEEE Photonics J. **11**, 1–12 (2019). Copyright 2019 Author(s), licensed under a Creative Commons Attribution (CC BY) License.

allows accessing the generation at the short wavelengths edge of the SWIR range. The suppressing, of otherwise, the dominant long-wavelength gain (>1.8 μm) is achieved by utilizing its distributed short-pass filtering effect by the fiber bending technique.[69] More details can be found in Sec. III B.

2. Photonic crystal fibers. Light waveguiding in photonic crystal fiber (PCF) is obtained surrounding of the core with air capillaries, decreasing the effective refractive index. The arrangement of the capillaries enables a variety of desirable characteristics, which are not feasible in conventional fibers, such as "endlessly" single-mode operation, extremely large or small mode field diameter (MFD), and numerical aperture (NA),[70] as well as an intricate dispersion or birefringence tweak.

The architecture of PCF with large mode area could effectively mitigate detrimental nonlinearities. Therefore, Tm-doped PCFs enable the generation of ultrashort pulses with peak powers in the order of several hundreds of megawatt.[71] Owing to the advantage of large MFD, passive PCFs are exploited in schemes to generate high-energy femtosecond pulses via the soliton self-frequency shift in the short-wavelength edge of SWIR (1.7 μm window).[72]

Another role of a solid-core PCF is the induction of high-harmonic generation due to strong optoacoustic interaction between laser cavity modes and acoustic vibrations in the fiber core. The vibrations, therefore, act as a locking mechanism on the propagating pulses, enabling stable gigahertz pulse train at 1.85 μm wavelength range with low pulse timing jitter in TDFL.[73]

3. Novel materials: ceramics. Although silica glass is a great host material for rare-earth ions, at the SWIR spectrum, it exhibits some substantial obstacles, such as high phonon energy and resulting high losses, and a reduced lifetime of dopants at excited states. The well-refined drawing capabilities in recent years have expanded the range of processible materials. As mentioned before soft-glasses might be one solution, but the drawback is that they are hardly compatible with conventional silica fibers. At the same time, ceramics fibers allow better integration in the all-silica setup. Here, nanocrystals are dispersed into a glass fiber core, resulting in subtle variable properties. Various objectives can be pursued in this way, among those are a 40%-increase of thulium's quantum conversion efficiency extending the fluorescence lifetime of the $^3F_4$ manifold or a higher thulium concentration.[74,75] An increase of efficiency for frequency conversion like upconversion has also been reported.[76] The oxyfluoride glass-ceramic host, for example, provides high mechanical strength and low phonon energy due to fluoride nanocrystals.[77] However, the attenuation of these fibers remains in need of refinement. Currently, the SWIR range is not fully covered by active media beneath 1.7 and above 2.2 μm (see Fig. 1). Ceramic fibers offer additional dopants, such as Cr^{2+} for emission in the 2.2−2.6 μm range, which can become an object of intensive research and development.[78] Just now, the first silica-cladded Cr^{2+}:ZnSe core fiber laser has been presented.[79]

B. Saturable absorbers

Generally, mode-locking is initiated by discriminating lower laser fluence against higher fluence. Therefore, the first method for

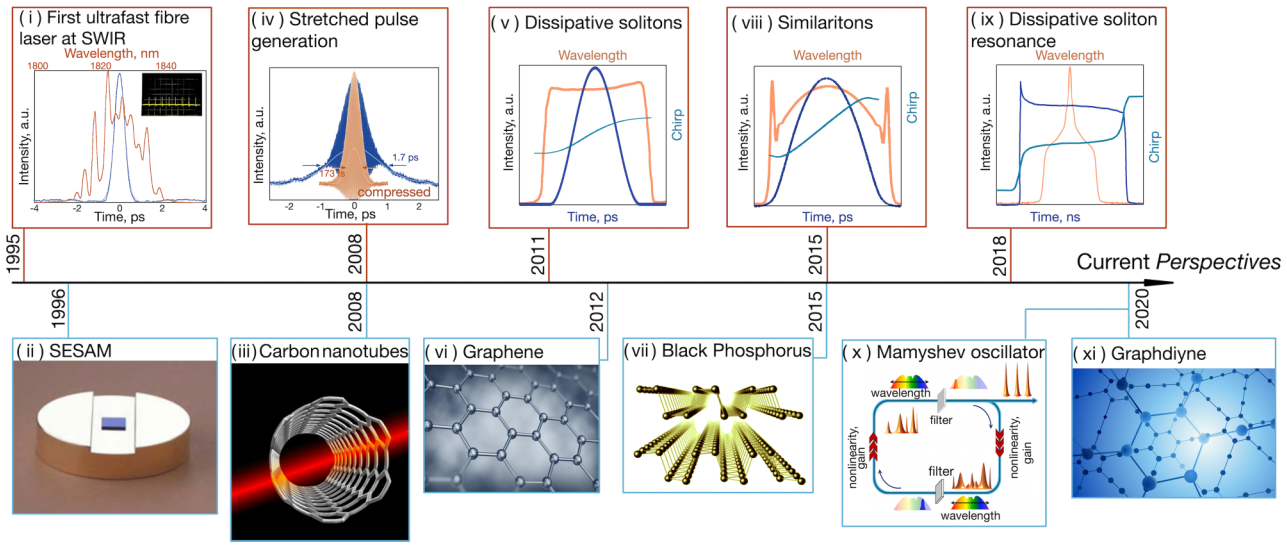

FIG. 4. Time line of demonstrated generation regimes and introduction of saturable absorbers in SWIR ultrafast fiber lasers.

its realization is by the incorporation of a special material in the laser cavity exhibiting nonlinear saturable absorption behavior. A second way to trigger mode-locking utilizes artificial modulators, exploiting the nonlinear optical Kerr effect and, therefore, intensity-dependency of the fiber-glass medium itself. It may be worth pointing out that in addition to these two passive approaches, there is also an active mode-locking with electronically controlled modulators. Still, since this technique leads to pulse duration in the picosecond range, we would limit our discussion to the former two approaches. Figure 4 reflects a timeline of the application of specific materials for mode-locking in the SWIR range.

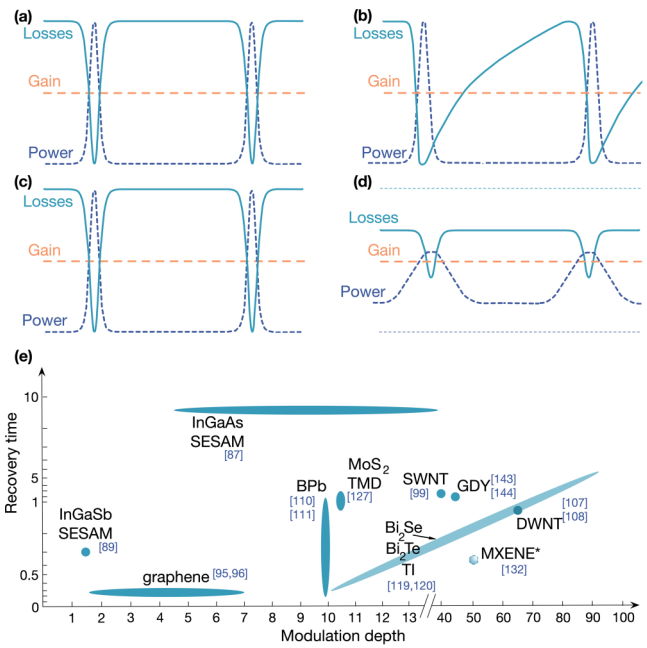

FIG. 5. (a)-(d) Mode-locking with different saturable absorbers: (a) fast and (b) slow relaxation time; SA with (c) high and (d) low modulation depth. (e) Summary of parameters of wide-spread SAs. *, the measurement of relaxation time has not yet been presented. The span of parameters corresponds to multi-layer structures.

An ideal saturable absorber (SA) has to feature a strong absorption in the non-saturated state (i.e., at low optical fluence) and a negligible absorption and scattering in the saturated state (i.e., at high fluence), giving virtually 100% modulation depth. The high modulation depth is encouraging a high signal to noise ratio, suppressing continuous wave breakthrough or phase fluctuation, as well as facilitates shorter pulses duration [Figs. 5(a)–5(d)]. A low necessary fluence to saturate the SA is beneficial for an efficient low power laser and generally for a low mode-locking threshold, whereas higher saturation fluence has been shown positive for high-power pulses. Another crucial requirement is a quasi-instantaneous relaxation time from saturated to non-saturated state. For this, most SAs are distinguished by two time constants, a fast and a slow.

1. Material saturable absorbers

Manifold available alternative materials with exceptional high third-order nonlinearity and rapid relaxation time have been proposed, including two-dimensional, atomic-layered semiconductors, such as graphene, transition metal dichalcogenide, as well as topological insulators and others. Unfortunately, up to now many of them have been presented without systematic comparative investigation of their fundamental properties as polarization sensitivity or long term stability reflecting their early stage of research, particularly, at the SWIR range. It should also be noted that many features of materials vary over different fabrication methods, preparations and geometries. Hence, properties are subject to significant

uncertainty.[80,81] In the current Perspective, we will discuss the most promising material SAs. Figure 5(e) allocates the majority of demonstrated material saturable absorbers against their two essential parameters, the modulation depth and the relaxation time.

1. Semiconductor saturable absorber mirror. The most mature and widely used SAs in commercially available ultrafast lasers are semiconductor saturable absorber mirrors (SESAMs), with quantum well structure mounted on Bragg mirrors. Pioneering works on ultrafast lasers in SWIR have demonstrated the high potential of SESAMs. Thus, the shortest reported pulses from a SWIR fiber oscillator attained 190 fs, 20 pJ, 50 MHz merely dated back in 1996.[82] Fiber-based SWIR lasers have demonstrated the generation of ultrashort pulses with a typical duration of ∼750 to 850 fs and energy ranging from 400 pJ to 1.6 nJ.[83–85] Unfortunately, the elaborate fabrication process of SESAMs through molecular beam epitaxy makes them comparably expensive and inflexible.[86] In order to adapt their narrow, ∼100 nm, operation wavelength to the SWIR spectrum and reduce relaxation time (typically of 10 ps[87]) several techniques haven been examined.[86,88,89] Particularly, InGaSb quantum wells placed near to the surface have been reported with a fast relaxation time of 300–500 fs,[89] 3–6% total loss,[90] and 1.5% modulation depth per quantum well. Yet, so far, this has been accompanied by the deterioration of other properties such as an increased defect density and corollary scattering loss due to non-suitable lattice matching. Accordingly, one has to weigh between recovery time and non-saturable loss.

2. Graphene. A monolayer of carbon atoms called graphene is distinguished by the shortest fast relaxation time of all pictured SAs with around 100–200 fs[91,92] and a zero bandgap, hence a high transmittance over a very broad spectrum.[93,94] On the downside stands a low modulation depth of approximately 1.8% per layer.[95,96] The modulation depth of structure with multiple layers increases proportionally but at the expense of the relaxation time and an increasing bandgap. Two to four layers have been reported to be an optimal thickness. Nevertheless, tens of layers, with 45% non-saturable loss, have been successfully employed, supporting the generation of 600-fs pulses.[97] Two-Photon-Absorption (TPA) is reported to be detrimental for high-power irradiating of graphene at the SWIR range, which limits its practical usage.[98,99] The implementation of graphene in a dispersion-managed holmium-doped all-fiber laser has ensured 1 nJ pulse energy within 190-fs pulsed generation.[100] The fabrication and handling of graphene are relatively straightforward procedures. Decent results have been achieved even with low-cost processes such as mechanical exfoliation. However, improvements in quality and yield of graphene production can be expected through the use of advanced techniques like chemical vapor deposition (CVD).[99] Durable substrates including metal, glass, and silicon are possible, leading to an admirable damage threshold about 2.7 TW cm^{-2}.[101]

3. Carbon nanotubes. The coiling of graphene into a cylinder with 0.6–2 nm diameter leads to the formation of carbon nanotubes (CNTs). CNTs feature a superb modulation depth and lower saturation intensity in the range from 10 to 60 MW cm^{-2} when compared to original graphene. In contrast, the longer fast relaxation time of around 1 ps[99] and an increased non-saturable loss have to be tolerated. TPA has been observed for near-IR but not for SWIR wavelengths. Many parameters are affecting the CNT properties as SA, such as diameter, chirality, length, functionalization, and orientation, which are predetermined by particular synthesis method and controlled in a subsequent post-processing step.[102] Particularly, the degree of the CNT orientation determines the polarization sensitivity of the SA.[103] For the operation at longer wavelength ranges, such as SWIR, CNTs diameters have to be larger, to match the bandgap. The diameter increase causes larger amounts of defects and loss increase, limiting maximum operation wavelength of single-walled CNTs (SWNT) to around 2.1 μm.[102] Alternative unique methods of SWNT fabrication, such as the aerosol (floating catalyst) chemical vapor deposition method,[104] allow extending their operational wavelength range up to 2.8 μm, preserving the quality of nanotubes with no defects.[105] A modified version of CNT consisting of a double-walled structure has been developed giving a 350 nm broad absorption around 1.9 μm,[106] 64% modulation depth,[107] and an almost halved relaxation time.[108] On the contrary, it stands a notable high 36% non-saturable loss and an even increased saturation fluence.[107] Their high surface energy brings about the possibility of agglomeration in the substrate, together with residual metal catalysts, which can lead to significant non-saturable losses.[98,109] In many reports, carbon nanotubes are embedded in a polymer for easy handling.

4. Phosphorene. Another aspirant attracting great interest is phosphorene, the layered version of black phosphorous. A monolayer features a relaxation time within the same range as graphene but with a higher modulation depth of roughly 10%. With multiple layers, the relaxation time increases together with the bandgap wavelength, which amounts 0.6−4 μm. An absorption, strongly dependent on polarization (98% degree of polarization), and a saturation fluence (2000 μJ cm^{-2}; 25 MW cm^{-2}) an order of magnitude higher than in graphene are on the downside.[110–112] Initial works have used hundreds of layers phosphorene for SA to achieve 10% modulation depth and 50% non-saturable loss. This allowed reaching up to 739 fs pulse duration in TDFL[54,113] and 1.3 ps in Ho-doped fiber lasers.[49] Owing to the environmental instability, phosphorene needs to be protected from oxygen, which causes complications during the fabrication process, post-processing, and subsequent usage. A relatively simple, inexpensive, and scalable fabrication method through inkjet-printing has demonstrated great potential, providing long-term stable SA samples.[114–118]

5. Topological insulators. Topological insulators (TIs) are characterized by a conducting surface and isolating interior, with Bi_2Te_3 and Bi_2Se_3 as the most prominent candidates. They possess a considerable modulation depth up to 95%,[119] a very low saturation intensity down to 1.1 W cm^{-2},[120] and a fast relaxation time up to 300 fs,[121] as well as a very broadband absorption well into the mid-IR.[122] It has been demonstrated that their SA properties can be adjusted by doping[123] and altering the number of layers. By increasing Bi_2Te_3 thickness from 8 to 16 nm, the modulation depth and the non-saturable loss increase from 14.5% to 65% and from 2.65% to 18.64%, respectively. At the same time, the saturation intensity decreases from 32 to 3.5 W cm^{-2}.[81] Their fabrication is possible with

a large uniform area, but it has been reported that the bandgap needs to be monitored after growing. The onset of TPA is not investigated in the SWIR for TIs. Regular results from TI mode-locked SWIR oscillators range about 800 fs pulse duration.[124–126] High-power versions have been presented only for the near-IR.

6. Transitional metal dichalcogenides. Unique materials consisting of one transition metal and two identical chalcogens are referred to as transition metal dichalcogenides (TMDs). They showcase a better saturable absorption than graphene per layer up to 10% and a moderate saturation fluence and loss, though a slightly extended fast relaxation time of 1–3 ps.[127] Despite TMDs feature comparable high bandgap, corresponding to the operational wavelength of 0.45–1.24 μm, by adjusting the number of layers in the structure, they are still able to operate in the SWIR spectrum. So far, the influence of TPA has not been studied. One remarkable example is the integration of MoS_2 as a butt-coupled mirror in a dispersion-managed, linear cavity resulting in the generation of 247-fs pulses with 15 nJ energy, or 150 mW average power, as well as 20% optic–optic efficiency.[128]

7. MXene. MXene is the newest emerged 2D-SA for the SWIR range, holding a bunch of promising characteristics. Its nonlinear absorption is two orders of magnitude higher than in black phosphorous or MoS_2[129] and it has a small bandgap wavelength of minimum 6 μm. A doubled damage threshold of 70 mJ cm^{-2} over a graphene sample has been shown.[130] Moreover, the thermal stability of MXenes varies according to their structure and chemical composition, such as Mo_2C_x or $Nb2CT_x$ are less thermally stable than a higher-atomic-layered $Ti_3C_2T_x$.[131] In the only demonstrated work for the SWIR, a remarkable high modulation depth of 49% and a pulse duration of 2.1 ps have been observed.[132]

8. Thermal stability enhancement for material saturable absorbers. For the integration in the laser cavity, the material SA conventionally is placed at the fiber ferrule facet. Thus, for use in transmittance, the SA is frequently sandwiched between two fiber connectors, while the SA mirror is simply butt-coupled. This uncomplicated yet crude procedure holds some disadvantages as it introduces a significant amount of loss by disturbing waveguiding. Hence, the SA should be as thin as possible, generally to tens of micrometers. Thus, in its turn limits the efficiency of light interaction with SA. Furthermore, to prevent Fresnel-losses, the SA has to be refractive-index-matched with the fiber connectors. Apart from these manageable limitations, the major one lays in low damage threshold due to incident high power light.

One circumvention to these constraints is to expose the SA only to the evanescent field of the laser. Whereas the interaction length is extended, typically, to few millimeters, a reduced fluence on the SA makes it more tolerant to high-power radiation. For implementing this idea, three major designs have been presented by using fiber (i) tapers or so-called microfibers, (ii) photonic crystal fibers, or by (iii) etching fiber cladding uniformly or only at one side, forming a D-shape cross section. These methods though introduce additional losses due to significant amount of leaking evanescent field. Also, enhanced nonlinear effects in a tapered fiber could be another concern. Some SAs are reported to be possible to disperse into the glass, which makes possible to integrate them in the cladding (of an active fiber) during fiber fabrication.[55,78,133] Therefore, the effective prolonged interaction of the evanescent field with SA will not be overshadowed by undesirable side effects.

While some of the nanomaterials mentioned above, particularly, carbon-based, have relatively high thermal damage threshold, embedding them in water-soluble polymers decreases damage threshold of resulted SAs (down to 0.9 mJ cm^{-2} for CNT-SA). The thermal degradation of surrounded materials is also enforced since carbon act as an excellent heat sink and transmit all energy to surrounding polymer.[134] Direct growth on a durable substrate, e.g., with SiO_2, can avoid such degradation and sufficiently improve the damage threshold.[105,135] Alternatively, inkjet-printing might be a possibility for efficient fabrication of single- or multi-material layer-stacks[117,136,137] with high thermal stability. Thus, graphene directly printed on the fiber tip has a damage threshold of 200 mJ cm^{-2}, which is competitive with SESAM technology.

9. Prospects in material SAs. The sophisticated construction of SESAMs holds some techniques beneficial to transfer to the novel materials. Indeed, the frequently invoked advantages of SESAMs are not material inherent but stem primarily from an ingenious design. For example, an antireflection and cap layer may increase the damage threshold and decrease losses, whereas a Fabry–Pérot sub-cavity can boost the modulation depth. Further enhancement can be seen in the combination of different SA material layers to compensate for their complementary advantages and disadvantages. Particularly, antimonene,[138] bismuthene,[139] metal organic frameworks, noble metal dichalcogenides,[140] perovskite,[141] and quantum-dot versions of those materials are not yet demonstrated in the SWIR spectrum.

It is also of seminal relevance that with the aid of CNTs and graphene modulators like SAs with electrically tunable optical response have been constructed enabling ultrafast lasers with online controllable operational regimes.[105,142]

As we mentioned above, more and more novel materials exhibiting nonlinear response are emerging. These include highly promising all-carbon nanomaterial, graphdiyne (GDY), which has recently demonstrated direct natural bandgap, broadband nonlinear absorption, high optical and chemical stability, ultrafast relaxation time, and low saturation intensity. Initial works have proved the potential of GDY for application in ultrafast photonics.[143,144]

It is also worth noting 2D plasmonic-based metasurfaces based, generally, of gold nanorods, are gaining more and more research attention. Together with their remarkable nonlinear absorption and broadband operation,[145–147] surface design (size, gap, and orientation) provides unusual polarimetric nonlinear transfer functions.

2. Artificial modulators

The second approach to trigger mode-locking is by utilizing the nonlinearity of the fiber medium itself, i.e., by triggering the nonlinear optical Kerr effect. It posses a supreme relaxation time of around 5 fs, the highest damage threshold, determined by damage threshold of optical fibers. Although these modulators can be treated as wavelength-independent, the lower effective nonlinearity of silica fibers in the SWIR range compared to the near-IR affects

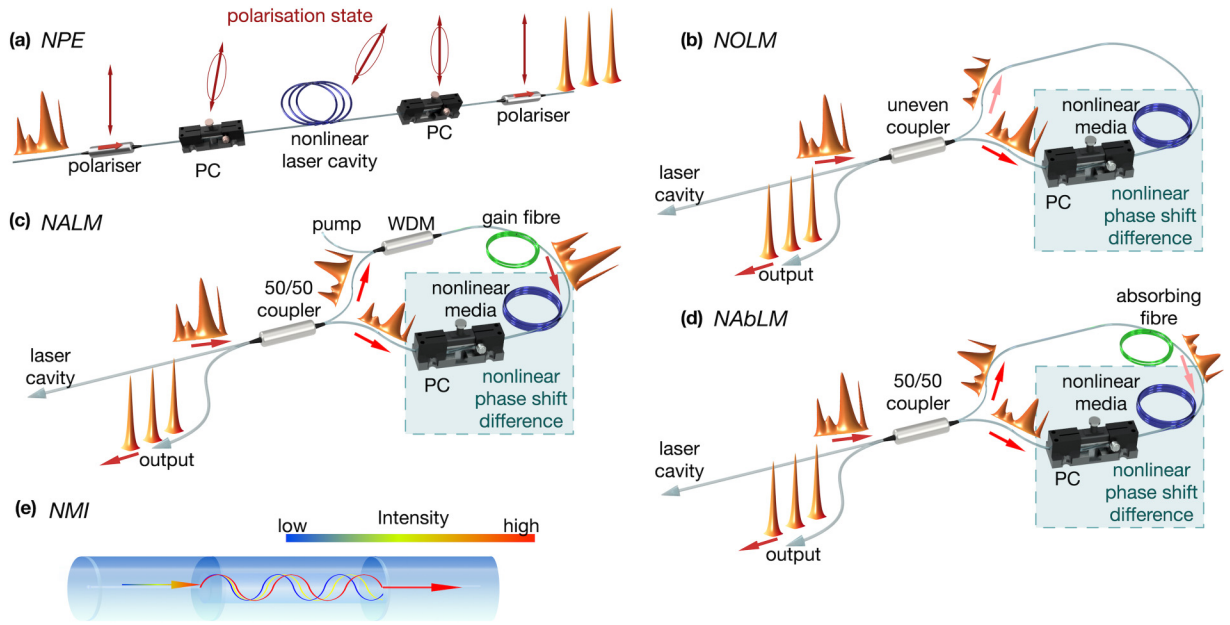

FIG. 6. Principles of artificial modulators. (a) Nonlinear polarization evolution (NPE); (b) nonlinear optical loop mirror (NOLM); (c) nonlinear amplifying loop mirror (NALM); (d) nonlinear absorbing loop mirror (NAbLM); and (e) nonlinear multi-modal interference (NMI). PC: polarization controller.

the nonlinear response and impose higher mode-locking threshold than with material saturable absorbers. The operational principles of the modulators are summarized in Fig. 6.

1. Nonlinear polarization evolution. Passive mode-locking can be initiated due to nonlinear polarization evolution, which is caused by intensity-dependent (nonlinear) change to the elliptical polarization state. Due to the difference in intensities, orthogonal polarization states obtain a different turn in the refractive index caused by the nonlinear optical Kerr effect. A general NPE realization contains polarization-selective components, of which transmission state is tuned to minimize losses for higher intensity components and maximize absorption of the lowest ones [Fig. 6(a)].

To the detriment of stability, research frequently applies an assembly of free-space bulk polarization isolator and retardation plates. More user-friendly implementations involve pig-tailed versions of those, like polarization-dependent in-line isolators[148] or hybrid wavelength-division-multiplex-isolator devices,[149] delivering still up to 143 fs, 31 nJ, 370 mW at 1950 nm. Indeed, truly fiberized oscillators have been obtained utilizing filters based on polarization-maintaining-fibers (PMFs),[150] tilted[151,152] or chiral[153,154] fiber Bragg gratings (FBGs), and evanescent field coupling.[95,155,156] Up to now, NPE mode-locking has been presented by just coiling a short piece of bend-sensitive fiber.[157]

2. Nonlinear loop mirrors. The principle of operation of nonlinear loop mirrors (NLM) relies on an asymmetrical Sagnac interferometer, interfering destructively for low fluence input. By leveraging self-phase modulation, only a higher fluence pulse undergoes enough phase shift for constructive interference. To break the symmetry of the counter-propagating pulses in the Sagnac loop, nonlinear optical loop mirrors (NOLMs) use an uneven splitting ratio of the forming coupler[158] [Fig. 6(b)]. When extra active fiber is used, the Sagnac interferometer is referred to as nonlinear amplifying loop mirror (NALM)[159][Fig. 6(c)]. Implementation of highly dispersive and nonlinear fibers allows improving the intensity selectivity of the loops.[160,161]

The accomplished pulse duration by NLM is usually slightly longer than by NPE, whereas the reliability is predominant to NPE and inferior to material SAs. Carefully designed, as with NPE, it suppresses the dispersive waves.[162] Ordinarily, yet not mandatory, released NLM-based oscillators comprise more fiber-optic components and a more extended cavity compared to NPE mode-locked ones. The used coupler determines the damage threshold.

The implementation of loop mirrors in the SWIR range is quite seldom,[30,163,164] nonetheless, reported performances amount to pulses duration and energy of 682 fs, 8.75 nJ,[40] or up to 424 fs and 65 nJ.[165] The realization of an all-fiber, all-PM version for the sake of more excellent environmental stability is simpler with NLM than with NPE.[52,166] Recently, the new type of NLM has been reported, where mismatch of the intensities of the counter-propagating beams in a loop is created not by gain but additional non-saturable losses[167][Fig. 6(d)].

3. Combination of techniques. Both material and artificial SAs have demonstrated their advantages and shortcomings. Thus, material SAs facilitate longer pulse durations and feature a

lower damage threshold and may degrade with time; however, they have a low self-starting threshold for ultrashort pulse generation. While artificial modulators, based on nonlinear optical Kerr effect, enable the formation of high-quality pedestal-free ultrashort pulse formation, they often do not exhibit self-starting anymore bearing lower nonlinearity at SWIR.

With the combination of both types of mode-locking techniques, the material saturable absorber can initiate and stabilize pulse formation, whereas the pulse width can be shaped and cleaned with the artificial saturable absorber to shorter durations. Furthermore, the constraints of the phase shift in a well-functioning NPE cavity are relieved.[169]

There are vigorous investigations on this scheme combining various kinds of SAs in TDFLs[31,170–173] and also in a Ho-doped fiber laser.[174] On the other side, some materials, as TIs, can act as both SAs and polarizers to enable the NPE. Such joint operation of a single device presents a promising approach for transferring to the SWIR.[32]

Typically, a combination of saturable absorbers and modulation technique results not only in better output parameters than a solitary one but reveals new operational modes. Thus, Ref. 168 demonstrated a ring laser with additional S-shaped feedback. In such a design, the pulse formation was enabled by two loop mirrors and assisted by CNT-SA (see Fig. 7). The resulting isolator-free NOLM–NALM-based, or so-called "Yin-Yang," schematic demonstrated switching of the direction of the laser generation or generation of two synchronized pulse trains by adjusting the output coupling ratios and thus altering the reflection of loop mirrors.

4. Prospects. After its prediction in 2013[175] and various implementations in the near-IR, lately, the nonlinear multi-modal interference mode-locking technique (NMI) has also been translated for the SWIR regime[176][Fig. 6(e)]. This SA-method impresses by its simplicity incorporating just a composition of graded- or step-index multi-mode fibers in-between the single-mode fiber. Here, the length of multi-mode fiber is chosen to correspond to the self-imaging length of a high-intensity pulse, differing by dint of the Kerr effect from lower intensities. Hence, lower intensities are filtered out at the junction of multi-mode to single-mode fibers.[175,177] Noteworthily, this method belongs to a broader class exploiting nonlinear mode-coupling.[178,179]

Very recent results show advanced characteristics through tapering[180] or coiling[181] giving 22% modulation depth, which is an almost comparable value to the behavior of NLM with 30% and 60% for the modulation depth and non-saturable loss, respectively.[161] Notwithstanding, unlike for the near-IR,[182] only pulses durations of roughly 1 ps have been realized for TDFLs, up to now.[173,183]

The mode-locking mechanism, based on Faraday instabilities, has drawn extensive research attention in the previous couple of years. In Mamyshev oscillator, two spectrally detuned filters exclude monochromatic CW oscillation. However, once a high-intensity pulse, as in the mode-locked state, provokes enough spectral broadening by self-phase modulation that it spans the spectral offset, a self-sustaining oscillation is permitted.[184,185] Depending on the ratio of spectral offset and nonlinearity, a substantial rectangular modulation depth has been proved to enable higher energy pulses compared to previously discussed SAs for near-IR setups. Still, on the other hand, it hinders self-starting behavior. Joining both features remains a challenge. The only SWIR implementation features moderate pulse energy of 3.5 nJ, 53.4 mW average power and 208 fs compressed duration. Nevertheless, the latest Tm-doped Mamyshev laser had to be seeded externally for starting.[186] Simple design and good tolerance to environmental perturbations, gain bandwidth and nonlinear phase accumulation renders the Mamyshev oscillator a promising concept. However, much effort is still ahead in solving shortcomings for SWIR lasers.

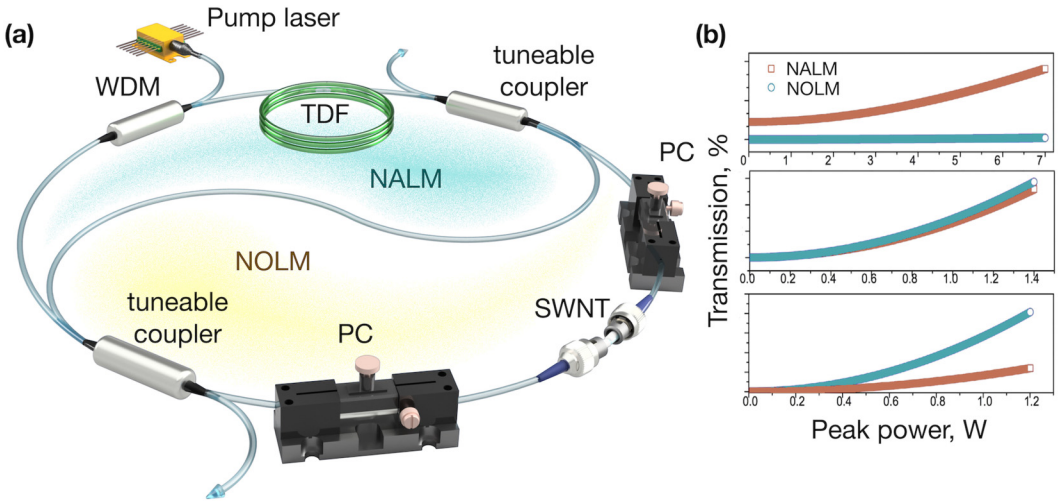

FIG. 7. Yin-Yang laser configuration: (a) schematic; (b) NOLM/NALM transmission tunability (output switching) at different coupling ratios. Adapted from Chernysheva *et al.*, Sci. Rep. **6**, 24220 (2016). Copyright 2016 Author(s), licensed under a Creative Commons Attribution (CC BY) license.

III. HIGHLIGHTS OF TM-DOPED MODE-LOCKED LASERS

As it was already mentioned above, silica-based TDFLs have demonstrated generation in the wavelength range spanning from 1.63 to 2.2 μm with different oscillator configurations and up to 300 nm tuning range could be achieved within a single configuration.[187] High repetition rates of up to 2.7 GHz,[188] as well as 10-fs pulse durations and energies up to 10 μJ[189] have been realized in all-fiber Tm-doped laser systems. However, there are still continuously growing demands on output flux, beam quality, tunability, and stability, particular for all-fiber versions. These challenges are identified in addition to obstacles and countermeasures reaching the edges of the SWIR.

A. Operational regimes

In this subsection, we review the major pulse regimes in mode-locked TDFLs, with an emphasis on the use of silica-based TDFs. Figure 4 demonstrates the timeline with first demonstrations of particular regimes together with a schematic representation of the temporal and spectral profile of generated pulses. In ultrafast fiber lasers, pulse formation relies on the balance of self-phase modulation (SPM) and group-velocity dispersion (GVD), as well as the amplitude modulation from the spectral filter or saturable absorber. Due to the position-dependent GVD of different components in a laser cavity, a "dispersion map" is literately created to categorize the operational regimes of ultrafast fiber lasers. Figure 8 presents the generation regimes defined by the cavity dispersion and highlights of their state-of-the-art performance.

1. Soliton generation

For a basic approach, a local compensation, the dispersion must be anomalous and the Kerr effect positive so that the phase shift caused by the former is just compensated by the latter, forming a temporal optical soliton. The optics community assigns soliton pulses as to stationary solutions of the cubic Ginzburg–Landau equation, which has to satisfy two conditions, the first of which is to feature a hyperbolic secant pulse shape. Second, the peak power and pulse duration are subject to the ratio of average dispersion and non-linearity: $E_s \propto |\beta_2|(\gamma \cdot \tau_p)$, thus fulfilling soliton area theorem.[190] It means that the pulse energy E is not arbitrarily scalable, yet limited by the laser cavity parameters.

Here, we have an asset in the SWIR range since silica glass has a high anomalous dispersion compensated by comparatively small effective non-linearity. In this regime, the maximum reached average power of solitons from all-fiber Tm-doped oscillators lies at impressive 300 mW with 1.28 ps (600 fs) pulse duration and corresponding to 4.06 nJ (2.93 nJ) pulse energy (not accounting dispersive waves) and 32.6% optic–optic efficiency.[171] Yet, the pulse energy rarely exceeds 1 nJ.[30,62,85,102,166]

A simple approach to reduce the nonlinear phase accumulation is to incorporate fluoride glass or large mode area fibers (LMA) TDF, which allowed to achieve soliton with an exceptional pulse energy of 4.5 nJ.[33] However, LMA fibers in ultrafast lasers tend to sacrifice all-fiber benefits of robustness to environmental perturbation, ease of constructing and integration. Besides, typical ps and sub-ps pulse duration (with recorded shortest 100 fs) in the soliton regime is limited by the inherent anomalous GVD.[34] A femtosecond pulse is achievable in an ultrashort cavity design exhibiting small anomalous GVD, which could be realized by implementing hybrid fiber components.[35,36]

2. Dispersion managed soliton generation

The limitations of soliton lasers in terms of pulse energy and duration can be mitigated in the dispersion-managed cavity. Here, segments of near equal normal and anomalous GVD are alternating in a laser cavity to create a "breathing" pulse dynamic, periodic pulse broadening and compression over a round trip. Thus, with the extending of its duration, the pulse peak power is significantly reduced, and it accumulates less nonlinear phase, allowing an increase of the pulse energy. The pulse evolving in the near-zero cavity dispersion is called the dispersion-managed (DM) soliton.

As discussed above, silica exhibits large anomalous dispersion at the SWIR spectrum. Therefore, normal dispersion fibers for this task have to be specially designed. Such fibers typically have a quite small core and, thus, introduce higher nonlinearity and additional losses when spliced to standard fibers.[39,64] Therefore, chirped FBG or free-space gratings present an attractive alternative for dispersion

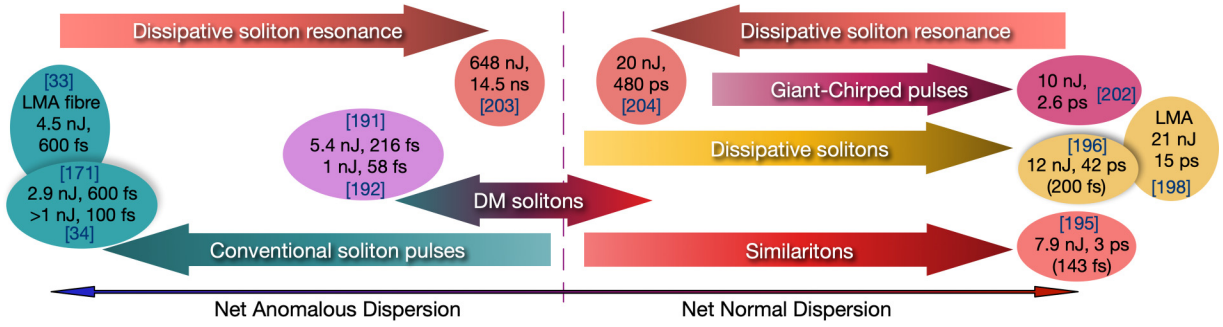

FIG. 8. Summary of mode-locked Tm-doped fiber laser operation regimes sorted by net dispersion, including the respective state-of-the art results of pulse energy and pulse duration. Here, DM solitons: dispersion managed solitons.

management, thus that the pulse energy could be scaled to 5.4 nJ in a free-space assembly.[191]

A net-cavity dispersion around zero to a slightly normal show best performances, but further power scaling is limited by the onset of multi-pulse instability when the nonlinear phase shift reaches roughly π. Applying this scheme followed by nonlinear compression, sub-100 fs DM soliton can be generated in a near-zero dispersion cavity.[192] The laser cavity with a $\sim 0.017\,\mathrm{ps}^2$ net GVD has generated a 58 fs, 1 nJ DM soliton at 1920 nm after the compression in dispersion compensation fiber.[193]

3. Self-similar evolution

Similaritons, or self-similar pulses, have quadratic (parabolic) temporal intensity distribution and a linear chirp, i.e., quadratic phase shift. Similaritons preserve their shape (yet not the pulse duration) during propagation in a long normal dispersion medium with sufficient amplification. Such self-similar evolution is explained by the SPM induced parabolic spectral and phase changes together with the quadratic phase shift in the frequency domain caused by normal dispersion of the medium. Therefore, the shape of the pulses after propagation is determined by seed pulse energy but not the shape or duration of the initial pulses. In such a case, every input pulse might obtain a parabolic profile, but the fiber parameters would then define pulse parameters. As an essential condition, a finely matched spectral filter is required to restore the pulse width after a round trip. Similariton generation is attractive in a short pulse laser due to its high tolerance of unlimited nonlinear phase shift and the staving off wave breaking. Besides, the monotonic frequency chirp across similariton enables a shorter compressed pulse.

High energy (>30 nJ) passive self-similar pulses at SWIR are theoretically possible using short length anomalous dispersion TDF.[194] Demonstration of similariton generation has been thus far quite uncommon since it is more challenging to achieve compared to DM or dissipative solitons due to the critical requirement of spectral filter. One of the rare works has reported on the similariton-like pulse generation with the pulse energy of 7.9 nJ.[195] Evolution of pulses with arbitrary shape into similaritons can be facilitated by applying optical fibers with increasing normal dispersion, including conical tapered fibers.

4. Dissipative soliton generation

As was mentioned above, while it is complicated to achieve self-similar propagation, the non-parabolic pulse can be stabilized under the condition of normal dispersion broadening. As SPM broadens the pulse spectrum, it is possible to stabilize the pulse by introducing wavelength-dependent loss like a spectral filter or gain-narrowing and thus restoring spectral shape after a roundtrip. Additionally, a fast saturable absorber ensures that the pulse duration is confined after a roundtrip, particularly, when stabilizing from self-starting. This concept of dissipative soliton (DS) is first introduced in an all-normal dispersion configuration, where the balance of dissipative effects (gain, loss and spectral filtering) and conservative effects (GVD and SPM) leads to the characteristic steep-sided optical spectra.

Despite the anomalous dispersion of silica-based TDF, DS at the 10 nJ level at 2 μm could be generated in a net-normal dispersion cavity.[196] The maximum nonlinear phase shift in DS could be up to 10π, thus enabling much higher pulse energy than in case of conventional soliton pulses. To date, the pulse energy of DS at SWIR is typically a few nJ, which is limited by the large anomalous dispersion in active fibers compared with the counterpart at near-IR range. One approach to overcome this limitation and further increase the pulse energy beyond 5 nJ is by reducing the length but increasing the gain of active fibers.[197] Alternatively, the LMA TDF is exploited as in the soliton regime to achieve high-energy DS of 21 nJ at 2 μm.[198] Although the pulse duration of DS is typically in a few to tens of ps, it is possible to compress them down to less than 200 fs.[199–201]

A subset of this scheme is called Giant-chirp oscillator, where a magnitude of order longer passive fiber is used. Since the mode-locked repetition rate is directly linked to the resonator length, this approach can be used to increase the pulse energy. The giant linear chirp of these oscillators and a low repetition rate is additionally favorable for a downstream chirped pulse amplification (CPA), making a pulse-picker and a stretcher, which introduces additional loss, dispensable.[202]

5. Other generation regimes

1. Dissipative soliton resonance. (DSR) also exhibits a phenomenon of free wave breaking in both net normal and anomalous dispersion regimes, and typically tens of nanoseconds pulses are achievable with the pulse energy up to hundreds of nanojoules. However, DSR exhibits low pulse peak power.[203,204]

2. Noise-like pulse. It is worth mentioning that the noise-like pulse (NLP) with a femtosecond coherent spike is not limited by the anomalous dispersion of TDF, with high energy achieved at 2 μm in both anomalous dispersion and normal dispersion cavity.[199,205] Moreover, the amplified NLP with energy above 50 nJ at 2 μm could serve as a pump source for mid-IR supercontinuum generation.[206]

3. Multi-pulse operation. It can occur in a laser cavity due to over-driving of mode-locking mechanisms, generally, happen with the significant increase of the pulse energy above the fundamental limit (see Sec. III A 1). In such a case, soliton energy quantization leads to the pulse splitting, including generation of soliton molecules,[107,207] soliton bunching,[55,208] or harmonic mode-locking.[49,209,210]

4. Two-color generation. In order to provide sources for SWIR dual-comb spectroscopy, single ultrafast oscillators can be triggered to emit two colors simultaneously.[107,211] This is enabled by employing a periodic filter, two transmission peaks of which lay in the gain spectrum. Often fiber lasers based on nonlinear loop mirrors are capable of operating in dual-wavelength generation regime. A simple free-running example delivers generation of several mode-locking states with central wavelengths, separated by 63 nm with a frequency stability better than 3.7×10^{-5}.[212] A bi-directional mode-locked ring TDFL is another demonstrated method, which enabled tunability of the central wavelength of counter-propagating pulses from 5 up to 35 GHz.[213]

6. Few cycles pulses

As aforementioned, intense laser pulses with just a few electromagnetic wave cycles—one cycle corresponds to 6.7 fs at 2 μm—have become a backbone of modern fundamental laser research, awaiting to be expanded by the SWIR spectrum. While the shortest laser pulses directly from an oscillator are obtained with a TDFL and amount to 58 fs, 1 nJ at 500 MHz repetition rate, the majority of novel high-power pulses barely reach 100 fs. With a pre-chirped pulse oscillator and a downstream compression line, which is either a fiber, a chirped FBG or mirror, or a free-space grating assembly of opposite dispersion, 80 fs pulse duration has been attained, limited due to non-matched third-order dispersion.[214] With thulium's saturated gain bandwidth, there is only a little space for further improvement. Hence, one takes advantage of spectral broadening by SPM in an external nonlinear compressor. Here, (gas-filled) PCFs or solid highly nonlinear fibers from germanium or chalcogenide are utilized as nonlinear media. Then there are different viable external compression schemes. Solitonic nonlinear self-compression combines spectral broadening and temporal compression in a single anomalous dispersive fiber. The pulse quality is degrading with increasing compression ratio; thus, one of the mitigation strategies is to distribute on multiple stages or use of speciality fibers. For instance, feeding high-power ultrashort pulses from a free-space, rod-type-fiber thulium CPA to a gas-filled antiresonant hollow-core fiber has enabled the generation of 13 fs pulses with 34 μJ pulse energy at 1820 nm, as well as 9-fs pulses with 102 μJ at 1730 nm.[215,216] When resorted to a solid fiber as compressor, SWIR pulses with 24 fs and 25 W average power has been demonstrated.[217] For making a compact system, the self-compression can be utilized in a single section of amplifier LMA-PCF, yielding in the generation of 20 W 50 fs pulses with 250 nJ pulse energy.[218]

A competing technique uses strong coherent spectral broadening by supercontinuum generation, Raman-shifted solitons or four-wave mixing in the first stage and linear compression in a subsequent. While the former approach captivates through a cost-effective design in a single fiber, the second allows for more freedom and hence shorter pulses in non-speciality fibers. A common way for the SWIR seeds a Tm-doped fiber amplifier (TDFA) with a non-linear broadened and wavelength shifted ultrafast erbium-doped fiber laser, whose output is compressed afterwards. Recently, a compact, all-PM-fiber frequency comb delivering 9.5 fs, 330 mW average powers at 100 MHz repetition rate has been reported, containing just commercial components.[214] The demonstration of a laser system based on thulium or holmium gain to reach the upper SWIR edge is still ahead of us, because of the high transmission loss and limited dispersion engineered fibers. Several attractive approaches have been suggested to streamline the generation of demanded broadband coherent spectra in the future, thus fostering lower required input powers. These include dispersion-decreasing or dispersion-oscillating fibers, tapered silicon core fibers as well as stretched flexible hollow fibers or all-normal dispersion chalcogenide PCFs.[219–222]

7. Prospects

Still, all those schemes suffer from the limited selection of normal dispersion fibers used in the SWIR domain, particularly, active ones, causing pulse breaking for high pulse energies. Currently emerging normal dispersive active fibers for the SWIR should enable to follow further improved concepts as the all-normal dispersion (ANDi) scheme or extended self-similar propagation, likewise gain-guided amplification. Nevertheless, this currently refers only to thulium-doped active fibers.

Nonetheless, normal dispersive fibers in the SWIR spectrum will presumably remain challenging and laborious to fabricate. Thus, it should be advisable to explore pulse propagation under anomalous dispersion further. The divided-pulse amplification scheme has been shown that it doubles the possible energy limit of a soliton pulse in a single stage, or increases it in several steps to 16-fold theoretically for the near-IR domain. Such an approach shows high potential for future enhancement mid-level SWIR systems in the anomalous dispersion regime.

While DSR pulses have a nonlinear chirp, their compression to the fs-duration with standard compressors has been reported. It is presumed that by use of nonlinear chirped FBGs or thin-film coatings, this value can be surpassed by several orders of magnitude. Therefore, DSR appears to be an auspicious direction for future increase of pulse energy, when appropriate normal dispersion fibers become available.

B. Short wavelength operation in TDF

As mentioned in Sec. II A, the broadband emission of Tm^{3+} ions in the $^3F_4 - {}^3H_6$ transition can cover the region from 1.6 to 2.1 μm. The wavelength region spanning 1600–1860 nm is of great importance for bio-imaging applications, where it offers deep penetration and high resolution (see Sec. IV). Despite the broadband operation, thulium-doped silica fibers feature strong reabsorption below 1860 nm between $^3F_4$ and $^3H_6$ energy levels. Therefore, to reach laser generation at the shorter wavelengths, shorter length of TDFs and, hence, higher doping concentration are required.[223] In addition, bulk filtering components are, generally, introduced into the stages of oscillator and amplifier to access the sub-1860 nm region.[224,225] For the chirped-pulse amplification system, reported in Ref. 225, femtosecond pulses with energy up to 20 nJ were achieved.

Compared with pure thulium-doping, Tm/Ho co-doped fibers provide higher gain below 1850 nm. Additionally, co-doping with Ho-ions provides a filtering effect due to its increasing absorption above 1850 nm. However, the pulse energy of the reported Tm/Ho-doped fiber-based lasers is still low in the soliton regime.[226] Another promising approach to reach is to use normal dispersion Tm:ZBLAN fiber and bulk component filter to achieve high pulse energy and ultrashort femtosecond pulse duration below 1860 nm.[227]

It is worth mentioning that above-discussed W-type normal dispersion TDF also enables access to shorter generation wavelengths as the W-profile exhibits a distributed long-wavelength filtering effect by fiber bending. All-fiber compact lasers with high pulse energy and short pulse duration at short wavelengths of 1852 nm and 1755 nm, respectively, were reported using a W-type NDTD[66,69] (Fig. 9). The progress of short wavelength ultrafast laser sources based on Tm fibers is shown in Fig. 10.

C. Power upscaling

A race for high-energy short pulses in the 2 μm range has seen tremendous progress in the past decade due to the advancement in

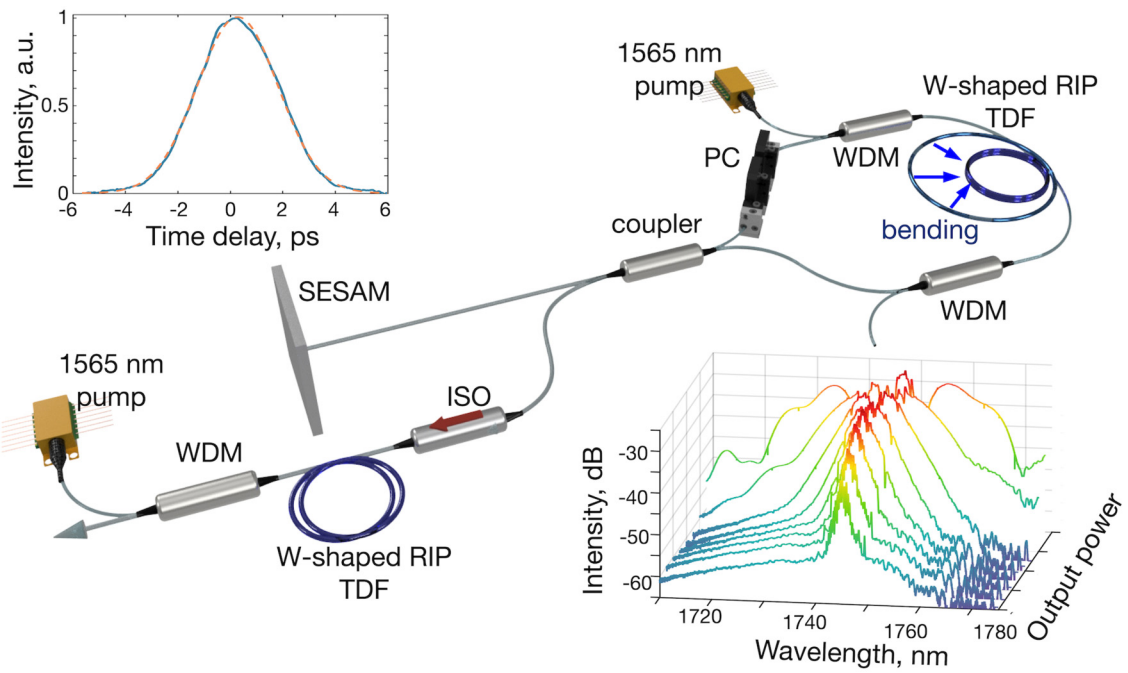

FIG. 9. Schematic of all-fiber mode-locked laser with normal dispersion TDF operating at short-wavelength edge of SWIR. Insets: Autocorrelation function and output spectra at different power. Adapted from Chen *et al.*, Opt. Express **28**, 17570–17580 (2020). Copyright 2020, licensed under OSA Open Access Publishing Agreement.

fiber design, materials and optical components. The encouraging factor here is also significantly reduced threshold for nonlinear effects and transverse-mode instabilities[228] due to longer generation wavelength, compared to Yb-doped fiber laser systems. Thus, theoretical[229] and experimental[230] studies have demonstrated that

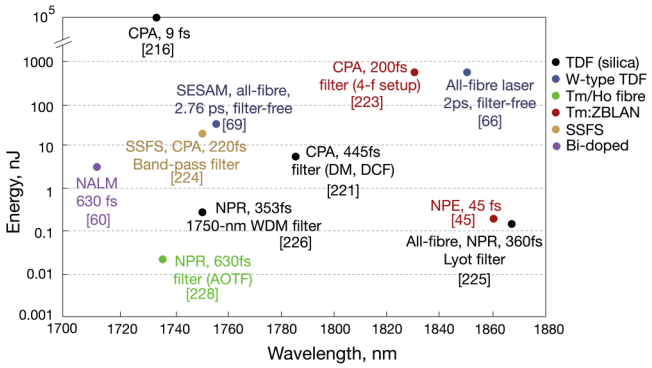

FIG. 10. Progress of ultrafast fiber laser in the short wavelength region. (SSFS: soliton self-frequency shift, SESAM: semiconductor saturable absorber mirror, CPA: chirped-pulse amplification, NPR: nonlinear polarization rotation, AOTF: acousto-optic tunable filter, WDM: wavelength division multiplexer, DM: dichroic mirror, DCF: dispersion compensating fiber.)

Tm-doped laser systems and amplifiers endure higher heat load at the threshold of thermal mode instability (95 W m^{-1} against 34 W m^{-1} for Yb-doped systems). A mode-locked pulse as short as 58 fs was generated at 1.925 μm from a TDF.[193] A cladding-pumped large mode area (LMA) TDF was selected for high-energy scaling. Ultrafast pulses with 21 and 52.4 nJ pulse energy were generated in an oscillator, for single-mode and few-mode operations, respectively.[198,231] A cladding pumping scheme using LMA fibers is increasingly used in the 2 μm region.[40,198,231] While pulse energy can be increased in this manner, additional dispersion control is required to generate shorter pulses. For instance, achieving sub-50 fs pulses is difficult due to the largely anomalous dispersion of silica TDFs and SMF-28 used in a cavity. For reaching sub-50 fs pulse duration, nonlinear pulse compression schemes were demonstrated relying on highly nonlinear fibers, gas-filled hollow-core fibers, or the Kagome photonic crystal fiber (PCF).[192,214,232] The nonlinear scheme was able to produce state-of-the-art results, including 9.5 fs pulse.[214]

In virtue of the chirped-pulse amplification (CPA) technique and LMA fibers, the acquirable performance level can drastically increase. A typical single-pass compressor efficiency amounts to ~80%, despite generally applied pulse pickers causing additional losses. A laser's future application determines whether a high average or peak power is desirable. Conventional solid LMA fibers can provide core sizes up to 25 μm, allowing all-fiber thulium CPAs, including compression and stretching within chirped Bragg gratings with 11 MW peak power in 530 fs pulses.[189,233] In a partly

free-space setup with three amplifiers, the peak power could be boosted to 200 MW with 15 W average power, albeit a 20% optic–optic efficiency.[234]

In order to achieve even higher performances, free-space systems with LMA-PCFs currently present the only solution. An average power of up to 1 kW within 265 fs duration corresponding to 50 MW of pulse peak power by admirable 60% optic–optic efficiency has been demonstrated.[235] Indeed, the highest peak power of 11 GW[216] is achieved in few-cycles systems, but at the expense of average power. At the same time, a remarkably high 730 MW pulse peak power, together with 108 W average power of 250 fs pulses have been reported.[236] For shorter, 95-fs, pulses, peak power, and energy of 4.7 GW, and 0.4 mJ could be generated.[237]

Aspiring after superior performance levels, the coherent beam combining technique provides the possibility to combine several output beams of the above systems in one beam and, thus, multiply the available power. Initial work is also under way toward combining the output of multi-core fiber.[238] Even though such extensive systems are most likely to be used for research facilities, still, the above conventional methods offer plenty of potential for further development.

D. Prospects of specialty fiber development for power up-scaling

The prior works suggest power scaling benefits from a normal dispersion gain fiber, as also witnessed in the progress of Yb-doped fiber ultrafast lasers. We discuss prospects of further development of normal dispersion specialty fibers in Sec. II A 5. The extractable power in a fiber scales roughly proportional to the mode field volume. On the same, the threshold for detrimental non-linear effects as stimulated Raman scattering is raised. Consequently, steadily growing core sizes are sought after. Power scaling through a W-type fiber is fundamentally limited by reachable core size. The waveguide dispersion effect diminishes with a larger core due to enhanced mode confinement in a core. It is viewed that the core size of 5 μm is near the upper limit with core NA of 0.12 in the W-type fiber.[66] A straightforward step toward further power scaling would be employing an LMA fiber. Normal dispersion 2 μm LMA fibers were investigated through multi-component glasses. A germanate glass TDF was reported to have 20 μm core size.[239] The material could potentially provide normal dispersion in the SWIR region by using a step-index design.[240]

On the other hand, smart design can be introduced to realize silica-based LMA TDFs. Figure 11 demonstrates an example of LMA fiber with normal dispersion at 2000–2050 nm. The fiber is structured with a central doped large core surrounded by a ring of passive cores, to enable strong waveguide dispersion.[241] Figure 11(a) shows the measured refractive index profile, reflecting the increase of a mode area up to 340 μm^2 at 2 μm. Figure 11(b) demonstrates the calculated dispersion, which confirms a good coverage of the normal dispersion in the wavelength range around the 2 μm.

Over the last years, photonic crystal- and -bandgap LMA fibers have driven up the accessible power to amounts that were previously not even imaginable. However, the expensive and laborious production of such fibers and, more importantly, their non-flexible design

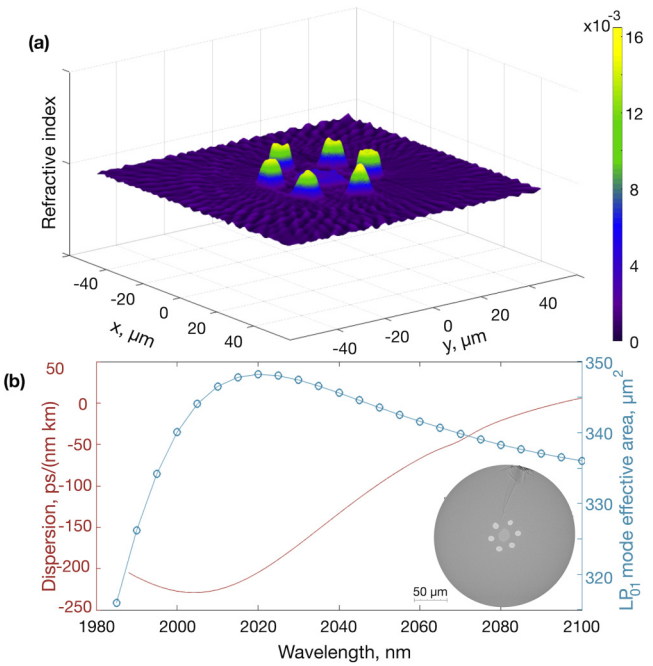

FIG. 11. Example of LMA dispersion shifted fiber produced at NTU, Singapore. (a) Refractive index profile; (b) calculated dispersion and LP01 effective mode area. Inset: Fiber cross section.

made them inconvenient for widespread all-fiber employment. Unfortunately, conventional solid LMA fibers with as large core areas are not single-mode anymore so that a common trend in the field is to depress higher-order modes (HOM), for example, by bending. Another feasible approach for overcoming this obstacle is by adding a third cladding around double-clad LMA fibers (i.e., development of triple-clad fiber) to disturb the shape of the undesirable modes[242] or elevate the degree of freedom in designing pump and signal propagation more independently. Recent advances in fiber drawing have shown that a manufacturing process named reactive powder sinter technology facilitates a more flexible production of larger, more uniform fibers over conventional MCVD.[244]

Further increase of core size by sustaining single-mode propagation has been shown by long-scale tapering such that one side is of the same size as single-mode fibers, while the other is of the multi-mode size. Demonstrated for near-IR range such normal dispersive single-mode fibers with up to 200 μm core diameter[245] would be very promising to investigate in the SWIR range, particularly, for self-similar propagation.

Another variant to preserve SM operation is by out-coupling HOMs evanescently into a second core, chirally winded around the central core (i.e., chirally-coupled-core fibers). Effectively single-mode core diameters of 50 μm could be implemented. Theses fibers have the advantage that they are fully solid and flexible. Even integrated fiber components like pump combiners are available so that chirally-coupled-core fibers may be acceptable to foreseen all-fiber systems on this platform also for the SWIR domain.[246]

E. All-fiber wavelength tunability

Numerous laser applications are driven by the ability to tune their frequency operation bandwidth. An adjustable intracavity wavelength-dependent loss together with a broad and favorably flat gain bandwidth and suppression of unwanted ASE are the principal criteria of emission wavelength tunability of ultrafast laser sources. These measures include the application of depressed cladding fibers or (dual-core) PCFs, co-doping with several active and absorptive ions, the advancement of pumping scheme by optimized saturation level bi-directional and multi-wavelength pump. The broadband gain spectra of thulium or Tm:Ho co-doped fibers have made the most significant contributions (see Fig. 12). Solely holmium-doped lasers have accomplished tunability spanning 2021–2096 nm[247] in the mode-locked regime or 2025–2200 nm in continuous wave operation.[248] Another critical aspect to be considered for some applications is rapid tunability up to a swept behavior, for which a short laser cavity is required. Still, this can result in facilitating substantial Q-switching instabilities.

A simple approach relies on angle shifting of diverse free-space, bulk components, including diffraction grating, volume Bragg grating, arrayed waveguide, or thin-film coating. Admittedly, the widest tuning range of an ultrafast SWIR laser spanning 300 nm from 1733 to 2033 nm has been demonstrated in Ref. 187. Nevertheless, the application of bulk components affects the environmental stability and exhibits substantial losses up to ∼5 dB. Fiberized versions of same components, when they are micro-opto-electro-mechanical integrated, have demonstrated almost the same range in a gain-switched regime.[249] At the same time, Fabry–Pérot filters, based on integrated gaped, mirrored fiber facets, have enabled tunability within 200 nm range. Nevertheless, high inherent losses of such systems, of about 2 dB, overshaded their applications. In contrast, Mach–Zehnder interferometer based filters attained ∼40 nm tuning with 0.6 nm resolution and high tuning speed by just 1.2 dB insertion loss.[250]

All-fiber solutions have been realized by applying birefringent Lyot-type filters for wavelength selection through adjustment of polarization controllers. Thus, a 143 nm tuning range has been demonstrated in NPE mode-locked TDFL,[223] 70 nm by applying a scheme with Sagnac loop, and 60 nm by using fiber tapers.[251] However, owing to the environmental dependent birefringence, precise, reliable and reproducible wavelength control is challenging to achieve. By bending, stretching, compressing, or tempering of multimode interference filters,[252] fiber Bragg gratings,[253] non-adiabatically pulled fiber tapers,[254] or photonic crystal fibers, a wavelength shift of 95 nm, 55 nm, and 50 nm have been obtained, respectively.

A virtually unlimited range can be received with an array of FBGs, even though a discrete tuning.[255] Using an acousto-optic tunable filter (AOTF) a fully electrically controlled 630 fs pulsed emission wavelength within the 1.7−1.8 μm range has been reported.[226] The free-space section might be avoided by applying the in-fiber AOTF technique, as demonstrated in *Hernandez et al.*.[256] First experiments have been shown that advanced materials, such as graphene- or CNT-SAs, as well as metal-coated fibers, possess great potential for electrically tuning.[105,142]

By nonlinear effects such as Raman soliton self-frequency shift or four-wave-mixing the emission wavelength and so the power is subordinated to the pump power. Unrestricted from a specific linear gain bandwidth, ultrashort pulses generation tunable over the entire SWIR band has been demonstrated.[63,65]

F. Noise suppression

Numerous approaches have been suggested to minimize amplitude and phase noise in a free-running fiber oscillator. Thus, the development of all-polarization maintaining fiber cavity architectures, the application of bandpass filters, enhancement of cavity Q-factor, or waiving of an extra-cavity amplification can substantially diminish amplitude and phase noise.[257] Advanced control of SAs parameters during fabrication can help reducing noise levels; thus, optimization of CNT and graphene oxide SAs allowed 10- and 8-dB reduction of phase noise in a TDFL, correspondingly.[258] Additionally, it has been demonstrated, that an external material SA, in particular, CNTs and graphene, acts as saturable phase noise

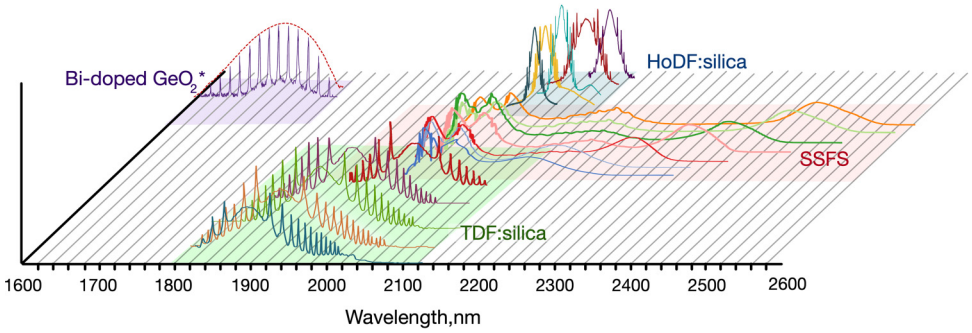

FIG. 12. Tunability range of SWIR fiber lasers. Adapted from Sun *et al.*, Opt. Express **25**, 8997–9002 (2017).[223] Copyright 2017, licensed under OSA Open Access Publishing Agreement; adapted from Chernysheva *et al.*, Nanophotonics **6**, 1–30 (2017). Copyright 2017 Author(s), licensed under a Creative Commons Attribution (CC BY) License and Firstov *et al.*, Sci. Rep. **6**, 28939 (2016).[243] Copyright 2016 Author(s), licensed under a Creative Commons Attribution (CC BY) License; adapted with permission from Koptev *et al.*, Opt. Lett. **40**(17), 4094–4097 (2015). Copyright 2015 The Optical Society.

suppressor.[259] Laser operational regime and wavelength also affect noise levels. Among the above-discussed generation regimes, fiber lasers operating at stretched pulse generation with net-cavity dispersion close to zero exhibits the lowest noise, while cavities with net-normal dispersion feature the highest noise.[257,260] Shifting laser generation wavelength far from the ASE peak allows decreasing the phase noise.[260] Following this, noise can be widely suppressed up to a technical noise floor from the pump and quantum ASE phase noise.[56,257,261] If even lower noise is demanded, one needs to stabilize through an electrical feedback loop.

So far, there is a relatively limited amount of research works reporting noise analysis in ultrafast SWIR fiber lasers. Relative intensity noise (RIN) of only 0.04% (integrated between 10 Hz and 10 MHz), yet time jitter of 1.705 ps, has been reported in a SESAM mode-locked TDFL operating at 1.6 GHz fundamental repetition rate.[262] Tm/Ho-doped fiber laser mode-locked by saturable Bragg reflector has demonstrated outstanding noise performance with a root mean square (RMS) intensity noise of 0.11% (integrated between 10 Hz and 2 MHz) together with a timing jitter of only 20 fs (integrated over a span from 100 Hz to 2 MHz).[56] Notably, an all-polarization-maintaining NALM design has proven remarkable performance. Thus, a HDFL with RMS RIN of 0.043% (integrated within 1 Hz–32.5 MHz span),[260,263] bringing them on the same performance level as advanced bulk counterparts. Recent advancements have enabled an exceptionally low integrated RIN of 0.047% (integrated between 10 Hz and 10 MHz) in an all-polarization-maintaining non-linear Tm-doped fiber amplification system with pulses of 96 fs, 350 mW at 100 MHz.[261]

IV. APPLICATIONS

The SWIR ultrafast fiber lasers can find niche applications that today's dominant 1 and 1.5 μm fiber laser cannot offer. Gas sensing is one of the few unique applications. The longer operational wavelength of SWIR lasers, at 2 μm and beyond, enables application for frequency comb-based free-space metrology like range finding, remote sensing and LiDAR as well as free-space, satellite optical communication. The SWIR lasers directly cover the resonance bands of O–H, C–O, and C–H bonds, which enables their applications for detecting such gases and vapors, as CO_2, N_2O, NH_3, CH_4, HF, HCN, and benzene or environmental, combustion, or process monitoring. A high spectral power (125 μW/nm) from an ultrafast laser at 2 μm was reported for atmospheric CO_2 detection after 2 m transmission.[264] In addition, several spectral features of minerals containing Si, Al, Fe, or Mg occur in the SWIR vital for geoscience.

Another application field includes industrial material processing and laser-induced breakdown spectroscopy of polymer, glass, diamond, and even metal with more pronounced absorption among the SWIR than in the near-IR. An enhanced tensile strength of welded polymers by 27 W TDFL exemplifies potential of the SWIR ultrafast lasers for such material processing with high precision.[265]

The ultrafast nature of generated pulses enables micromachining of the materials mentioned above with high precision, due to the relatively slow heat response rate of the materials compared to the laser pulse's time scale. A defect-free laser drilling achieved by 200 fs 120 μJ laser was compared to poor quality from a 3.3 ns 1 mJ pulse in the near-IR range.[266] Industrial interest in the high-power ultrafast fiber lasers, operating at SWIR range, is primarily driven by the possibility for micromachining of various non-metal materials, i.e., polymers and semiconductors. Most semiconductor materials are transparent in the SWIR, which promises three-dimensional selective micro-modification inside the wafer material or even at its back surface by ultrafast laser focusing, as reported in Ref. 267 using >100 kW peak power from a TDFL. The welding of semiconductors has found its application for microelectronics and photovoltaics. Notably, the possibility of silicon micromachining under its surface at 2.1 μm has made a significant impact on modern microelectronics. On the other hand, high absorption of polymers[268] in the SWIR implies energy-efficient processing (cutting, welding, marking, and engraving in a micro-scale) or laser deposition of polymer materials. For instance, an absorption coefficient of PMMA is ~1.3 cm at 2 μm, compared to negligible absorption at 1 μm, enabling precision cutting of only 11 μm width by using a 40 ps 1 μJ ultrashort pulse Tm-doped fiber laser.[268]

In the same vein, there is enormous potential in medical applications due to the strong absorption in the water at 1850–1930 nm range.[269] Coupled with small penetration depth, this means that bio-tissue, which is mostly water, can be processed with high precision. Medical procedures such as minimally invasive surgery, skin treatment, laser enucleating have the potential to acquire greater accuracy and reliability when using SWIR sources. A local absorption maximum of lipid in combination with a local minimum of water absorption around 1.73 μm enhances laser surgery of high-fat tissue against surrounding water-rich tissue. Besides, imaging techniques get a higher contrast.

Likewise, the wavelength in vicinity of 1.7 μm exhibit the lowest scattering in biological tissue, what reveals imaging techniques like optical coherence tomography, scanning near-field infrared microscopy, Raman spectroscopy or multiphoton imaging with utmost penetration depth.

Hence, the two-photon microscopy (2PM) using a 1300 nm light source experiences two–three times deeper penetration depth when compared to the 800 nm one-photon microscopy. In the aspect of the penetration depth, the deepest can be achieved by wavelength range around 1700 nm up to ~1300 μm depth, where three-photon microscopy (3PM) can be established.[72] Compared with the more conventional excitation wavelengths of 800 and 1300 nm, the 1700-nm sources can offer drastically reduced out-of-focus background noises, enabling orders of magnitude improvement of a signal-to-noise ratio (SNR).[22] Considering the inverse-squared relationship between generated fluorescence signal power and a repetition rate of a pulse train in the 3PM, an energetic (~100 nJ) and short (≫70 fs) pulse is required to realize the 3PM.[270] In addition, a low repetition rate (on the order of 1 MHz) is also required to avoid excessive sample heating.[72] Using a SSFS, a 65 fs 67 nJ pulse at 1675 nm was reported at a repetition rate of 1 MHz.[72] Also, a 150 fs Tm:ZBLAN fiber-based laser system delivering pulse energy of 1.1 μJ at a repetition rate of 1 MHz around 1.8 μm wavelength was demonstrated as a 3PM source.[271]

An all-fiber configuration would make the laser system compact, portable, maintenance, and alignment-free, and easily deployable in environmentally dirty industry settings. The output

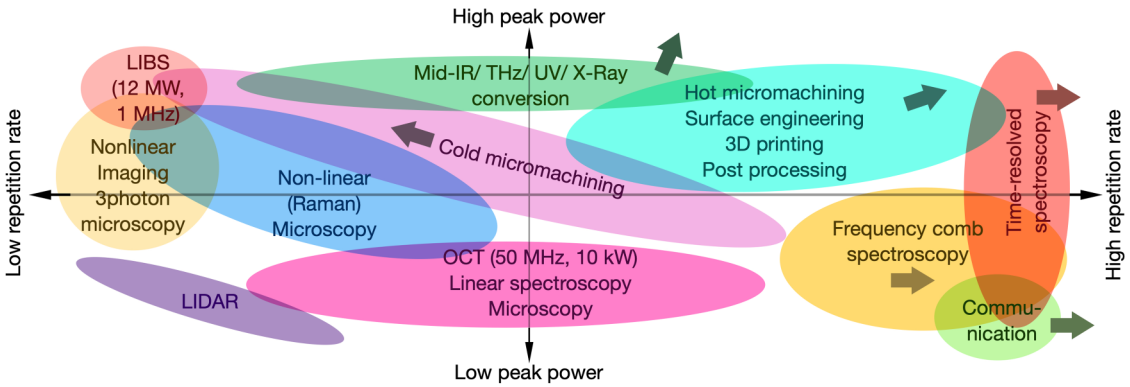

FIG. 13. Summary of application areas of ultrafast SWIR fiber lasers with according to the requirements on laser performance. Here, arrows indicate the direction for further improvement.

from fiber, especially a single-mode fiber, would mean that beam quality is nearly diffraction-limited and linearly polarized which improves the efficiency of the laser processing applications described.

Beyond that, at the short wavelength side around 1.65 μm one desires to expand wavelength-division-multiplexing in telecom optical communication, covering the U-band (1625–1675 nm) and bridging to the emerging 2 μm band. Originating from the advantage of longer wavelength for nonlinear frequency conversion, SWIR lasers are moreover appropriate pump sources to reach farther into the mid-infrared by optical parametric or difference-frequency generation, into the Terahertz range by optical rectification, as well as into the ultraviolet or x ray range by high-harmonic generation. As the cutoff photon energy (highest harmonic) is proportional to the square of the wavelength of the source, SWIR sources, as well as mid-IR, can increase the cutoff energy considerably.[272] For applications requiring supercontinua, such as hyperspectral imaging, several attempts have also been made laying on SWIR lasers as a pump source. A supercontinuum generation covering from 2 to 4.7 μm with an output power of ~7 W was generated in an InF_3 fiber using an actively Q-switched mode-locked Tm-doped fiber laser with 220 μJ total pulse energy.[273] A fiber with high germanium oxide concentration, whose zero dispersion wavelength lies at ~1.6 μm, can also be pumped by SWIR lasers for mid-IR supercontinuum generation.[274] Lastly, diligent research is conducted, among other things for medicine, on table-top laser-driven particle acceleration based on SWIR lasers.

Figure 13 summarizes applications discussed above and allocates them against their requirements on two of the key ultrafast laser parameters, peak power and repetition rate. The arrows here demonstrate where the progress in laser optimization should look for to fulfill the demands of the applications.

V. CHALLENGES AND PERSPECTIVES

To summarize, we believe that the SWIR ultrafast fiber lasers will undergo continued progress in future. Such enhancement is currently driven and will be undoubtedly further accelerated by numerous interesting excising and newly emerging applications. At the same time, the current major obstacle toward the rapid improvement of SWIR fiber systems is the limited selection of optical fibers and fiber-based components. This refers both to the lack of fibers allowing efficient dispersion and nonlinearity management and to availability of only a few special passive fibers, which, due to their design, provide multi-modal propagation for near-IR pump wavelengths. With further improvement of fiber fabrication techniques and unique fiber development, the forthcoming ultrafast SWIR sources have the full potential to outperform more mature laser systems operating in near-IR wavelength range, such as Ti:Sapphire or Yb-doped fiber laser, and allow reduction of the cost of such sophisticated ultrafast sources.

In the current Perspective, we have reviewed the current state of the art in SWIR ultrafast fiber lasers, generation regimes, pulse amplification, and system applications, including material micro- and nanomachining, medical diagnostics, telecommunication, metrology, and sensing (Fig. 1). All the diverse applications demand a variety of different laser designs to meet the requirements on pulses' bandwidth, shape, energy, peak power, and repetition rate. We identified current challenges and new vectors for laser system optimizations to tailor the output parameters to fulfill the whole range of the requirements and, thus, make applications more efficient and affordable. It is worth noting again that the most substantial part of the presented progress in ultrafast SWIR fiber lasers has been achieved only within the last decade. Therefore, we expect further output laser power upscaling, including via coherent combining in all-fiber systems, exploitation of higher-order dispersion pulse shaping, spatiotemporal mode-locking, Kerr nonlinear beam cleanup in multi-mode fibers, exploitation of numerous other techniques, and observation of new phenomena in the nearest future.

ACKNOWLEDGMENTS

S.Y. is grateful for the support by the Academic Research Fund Tier 1, Ministry of Education (Singapore) under Project Grant No. 2018-T1-001-148 (RG 84/18) and the Economic Development Board—Singapore (EDB) under Grant No. S16-1257-IPP COY-15-IPP/160006 in association with Sintec Optronics Pte. Ltd.

DATA AVAILABILITY

Data sharing is not applicable to this article as no new data were created or analyzed in this study.

REFERENCES

[1]R. R. Alfano and S. L. Shapiro, "Ultrashort phenomena," Phys. Today **28**, 30–37 (1975).
[2]A. McPherson, G. Gibson, H. Jara, U. Johann, T. S. Luk, I. McIntyre, K. Boyer, and C. K. Rhodes, "Studies of multiphoton production of vacuum-ultraviolet radiation in the rare gases," J. Opt. Soc. Am. B **4**, 595–601 (1987).
[3]T. Brabec and F. Krausz, "Intense few-cycle laser fields: Frontiers of nonlinear optics," Rev. Mod. Phys. **72**, 545–591 (2000).
[4]O. A. Hurricane, D. A. Callahan, D. T. Casey, P. M. Celliers, C. Cerjan, E. L. Dewald, T. R. Dittrich, T. Döppner, D. E. Hinkel, L. F. Berzak Hopkins, J. L. Kline, S. Le Pape, T. Ma, A. G. MacPhee, J. L. Milovich, A. Pak, H.-S. Park, P. K. Patel, B. A. Remington, J. D. Salmonson, P. T. Springer, and R. Tommasini, "Fuel gain exceeding unity in an inertially confined fusion implosion," Nature **506**, 343–348 (2014).
[5]A. H. Zewail, "Laser femtochemistry," Science **242**, 1645–1653 (1988).
[6]A. Mokhtari, P. Cong, J. L. Herek, and A. H. Zewail, "Direct femtosecond mapping of trajectories in a chemical reaction," Nature **348**, 225–227 (1990).
[7]C. G. Parthey, A. Matveev, J. Alnis, B. Bernhardt, A. Beyer, R. Holzwarth, A. Maistrou, R. Pohl, K. Predehl, T. Udem, T. Wilken, N. Kolachevsky, M. Abgrall, D. Rovera, C. Salomon, P. Laurent, and T. W. Hänsch, "Improved measurement of the hydrogen 1S–2S transition frequency," Phys. Rev. Lett. **107**, 203001 (2011).
[8]A. Beyer, L. Maisenbacher, A. Matveev, R. Pohl, K. Khabarova, A. Grinin, T. Lamour, D. C. Yost, T. W. Hänsch, N. Kolachevsky, and T. Udem, "The rydberg constant and proton size from atomic hydrogen," Science **358**, 79–85 (2017).
[9]M. DiDomenico, "Small-signal analysis of internal (coupling-type) modulation of lasers," J. Appl. Phys. **35**, 2870–2876 (1964).
[10]L. E. Hargrove, R. L. Fork, and M. A. Pollack, "Locking of He-Ne laser modes induced by synchronous intracavity modulation," Appl. Phys. Lett. **5**, 4–5 (1964).
[11]E. P. Ippen, "Principles of passive mode locking," Appl. Phys. B **58**, 159–170 (1994).
[12]A. Piper, A. Malinowski, B. Thomsen, D. Richardson, L. Hickey, and M. Zervas, "11.1 W average power, 20 ps pulses at 1 GHz repetition rate from a fiber-amplified gain-switched 1.06 μm Fabry-Perot laser diode," in *Conference on Lasers and Electro-Optics, 2005 (CLEO)* (IEEE, 2005), Vol. 2, pp. 1141–1143.
[13]J. J. Degnan, "Optimization of passively Q-switched lasers," IEEE J. Quantum Electron. **31**, 1890–1901 (1995).
[14]M. A. Gaafar, A. Rahimi-Iman, K. A. Fedorova, W. Stolz, E. U. Rafailov, and M. Koch, "Mode-locked semiconductor disk lasers," Adv. Opt. Photonics **8**, 370–400 (2016).
[15]P. Holl, M. Rattunde, S. Adler, S. Kaspar, W. Bronner, A. Bächle, R. Aidam, and J. Wagner, "Recent advances in power scaling of GaSb-based semiconductor disk lasers," IEEE J. Sel. Top. Quantum Electron. **21**, 324–335 (2015).
[16]C. Hönninger, R. Paschotta, M. Graf, F. Morier-Genoud, G. Zhang, M. Moser, S. Biswal, J. Nees, A. Braun, and G. Mourou, "Ultrafast ytterbium-doped bulk lasers and laser amplifiers," Appl. Phys. B **69**, 3–17 (1999).
[17]G. J. Koch, J. Y. Beyon, B. W. Barnes, M. Petros, J. Yu, F. Amzajerdian, M. J. Kavaya, and U. N. Singh, "High-energy 2 μm doppler LiDAR for wind measurements," Opt. Eng. **46**, 116201 (2007).
[18]C. Li, J. Shi, X. Gong, C. Kong, Z. Luo, L. Song, and K. K. Wong, "1.7 μm wavelength tunable gain-switched fiber laser and its application to spectroscopic photoacoustic imaging," Opt. Lett. **43**, 5849–5852 (2018).
[19]D. Grassani, E. Tagkoudi, H. Guo, C. Herkommer, F. Yang, T. J. Kippenberg, and C.-S. Brès, "Mid-infrared gas spectroscopy using efficient fiber laser driven photonic chip-based supercontinuum," Nat. Commun. **10**, 1–8 (2019).
[20]R. L. Blackmon, N. M. Fried, and P. B. Irby, "Comparison of holmium:YAG and thulium fiber laser lithotripsy: Ablation thresholds, ablation rates, and retropulsion effects," J. Biomed. Opt. **16**, 071403 (2011).
[21]S. Singh and G. Samuel, "Laser micromachining of semiconductor materials," in *Application of Lasers in Manufacturing* (Springer, 2019), pp. 111–141.
[22]D. G. Ouzounov, T. Wang, M. Wang, D. D. Feng, N. G. Horton, J. C. Cruz-Hernández, Y.-T. Cheng, J. Reimer, A. S. Tolias, and N. Nishimura, "In vivo three-photon imaging of activity of GCaMP6-labeled neurons deep in intact mouse brain," Nat. Methods **14**, 388–390 (2017).
[23]N. G. Horton, K. Wang, D. Kobat, C. G. Clark, F. W. Wise, C. B. Schaffer, and C. Xu, "In vivo three-photon microscopy of subcortical structures within an intact mouse brain," Nat. Photonics **7**, 205–209 (2013).
[24]M. Y. Koptev, E. Anashkina, A. Andrianov, V. Dorofeev, A. Kosolapov, S. Muravyev, and A. Kim, "Widely tunable mid-infrared fiber laser source based on soliton self-frequency shift in microstructured tellurite fiber," Opt. Lett. **40**, 4094–4097 (2015).
[25]Y. Tang, L. G. Wright, K. Charan, T. Wang, C. Xu, and F. W. Wise, "Generation of intense 100 fs solitons tunable from 2 to 4.3 μm in fluoride fiber," Optica **3**, 948–951 (2016).
[26]J. Wang, S. Lin, X. Liang, M. Wang, P. Yan, G. Hu, T. Albrow-Owen, S. Ruan, Z. Sun, and T. Hasan, "High-energy and efficient Raman soliton generation tunable from 1.98 to 2.29 μm in an all-silica-fiber thulium laser system," Opt. Lett. **42**, 3518–3521 (2017).
[27]T. Du, Y. Li, K. Wang, Z. Cai, H. Xu, B. Xu, V. M. Mashinsky, and Z. Luo, "2.01−2.42 μm all-fiber femtosecond Raman soliton generation in a heavily germanium doped fiber," IEEE J. Sel. Top. Quantum Electron. **25**, 1–7 (2019).
[28]S. Firstov, S. Alyshev, M. Melkumov, K. Riumkin, A. Shubin, and E. Dianov, "Bismuth-doped optical fibers and fiber lasers for a spectral region of 1600–1800 nm," Opt. Lett. **39**, 6927–6930 (2014).
[29]M. M. Kożak, *Development of Thulium-Doped Fluoride Fiber Amplifiers* (Cuvillier Verlag, 2005).
[30]C. W. Rudy, K. E. Urbanek, M. J. Digonnet, and R. L. Byer, "Amplified 2-μm thulium-doped all-fiber mode-locked figure-eight laser," J. Lightwave Technol. **31**, 1809–1812 (2013).
[31]M. Chernysheva, A. Krylov, P. Kryukov, N. Arutyunyan, A. Pozharov, E. Obraztsova, and E. Dianov, "Thulium-doped mode-locked all-fiber laser based on NALM and carbon nanotube saturable absorber," Opt. Express **20**, B124–B130 (2012).
[32]J. Bogusławski, G. Soboń, R. Zybała, K. Mars, A. Mikuła, K. M. Abramski, and J. Sotor, "Investigation on pulse shaping in fiber laser hybrid mode-locked by Sb_2Te_3 saturable absorber," Opt. Express **23**, 29014–29023 (2015).
[33]A. Sincore, J. D. Bradford, J. Cook, L. Shah, and M. C. Richardson, "High average power thulium-doped silica fiber lasers: Review of systems and concepts," IEEE J. Sel. Top. Quantum Electron. **24**, 1–8 (2017).
[34]M. J. Digonnet, *Rare-Earth-Doped Fiber Lasers and Amplifiers* (CRC Press, 2001).
[35]D. A. Simpson, G. W. Baxter, S. F. Collins, W. Gibbs, W. Blanc, B. Dussardier, and G. Monnom, "Energy transfer up-conversion in Tm^{3+}-doped silica fiber," J. Non-Cryst. Solids **352**, 136–141 (2006).
[36]S. D. Jackson, "Cross relaxation and energy transfer upconversion processes relevant to the functioning of 2 μm Tm^3+-doped silica fibre lasers," Opt. Commun. **230**, 197–203 (2004).
[37]B. Faure, W. Blanc, B. Dussardier, and G. Monnom, "Improvement of the Tm^{3+}: $^3H_4$ level lifetime in silica optical fibers by lowering the local phonon energy," J. Non-Cryst. Solids **353**, 2767–2773 (2007).
[38]W. Barnes and J. Townsend, "Highly tunable and efficient diode pumped operation of Tm^{3+}-doped fibre lasers," Electron. Lett. **26**, 746–747 (1990).
[39]S. Chen, Y. Jung, S.-U. Alam, D. J. Richardson, R. Sidharthan, D. Ho, S. Yoo, and J. M. Daniel, "Ultra-short wavelength operation of thulium-doped fiber amplifiers and lasers," Opt. Express **27**, 36699–36707 (2019).
[40]C. W. Rudy, M. J. F. Digonnet, R. L. Byer, and S. Jiang, "Thulium-doped germanosilicate mode-locked fiber lasers," in *Lasers, Sources, and Related Photonic Devices* (Optical Society of America, 2012), p. FTh4A.4.

[41]M. Tokurakawa, H. Sagara, and H. Tünnermann, "All-normal-dispersion nonlinear polarization rotation mode-locked Tm:ZBLAN fiber laser," Opt. Express **27**, 19530–19535 (2019).
[42]Y. Nomura and T. Fuji, "Sub-50-fs pulse generation from thulium-doped ZBLAN fiber laser oscillator," Opt. Express **22**, 12461–12466 (2014).
[43]Y. Nomura and T. Fuji, "Generation of Watt-class, sub-50 fs pulses through nonlinear spectral broadening within a thulium-doped fiber amplifier," Opt. Express **25**, 13691–13696 (2017).
[44]A. Hemming, N. Simakov, J. Haub, and A. Carter, "A review of recent progress in holmium-doped silica fibre sources," Opt. Fiber Technol. **20**, 621–630 (2014).
[45]A. Chamorovskiy, A. Marakulin, S. Ranta, M. Tavast, J. Rautiainen, T. Leinonen, A. Kurkov, and O. Okhotnikov, "Femtosecond mode-locked holmium fiber laser pumped by semiconductor disk laser," Opt. Lett. **37**, 1448–1450 (2012).
[46]S. A. Filatova, V. A. Kamynin, N. R. Arutyunyan, A. S. Pozharov, E. D. Obraztsova, P. A. Itrin, and V. B. Tsvetkov, "Comparison of mode-locking regimes in a holmium fibre laser," Quantum Electron. **48**, 1113 (2018).
[47]V. Dvoyrin, N. Tolstik, E. Sorokin, I. Sorokina, and A. Kurkov, "Graphene-mode-locked holmium fiber laser operating beyond 2.1 μm," in *The European Conference on Lasers and Electro-Optics* (Optical Society of America, 2015), p. CJ_7_4.
[48]J. Wang, J. Han, J. He, C. Liao, and Y. Wang, "High-energy mode-locked holmium-doped fiber laser operating in noise-like pulse regime," Opt. Lett. **44**, 4491–4494 (2019).
[49]M. Pawliszewska, Y. Ge, Z. Li, H. Zhang, and J. Sotor, "Fundamental and harmonic mode-locking at 2.1 μm with black phosphorus saturable absorber," Opt. Express **25**, 16916–16921 (2017).
[50]P. Li, A. Ruehl, U. Grosse-Wortmann, and I. Hartl, "Sub-100 fs passively mode-locked holmium-doped fiber oscillator operating at 2.06 μm," Opt. Lett. **39**, 6859–6862 (2014).
[51]M. Pawliszewska, A. Dużyńska, M. Zdrojek, and J. Sotor, "Metallic carbon nanotube-based saturable absorbers for holmium-doped fiber lasers," Opt. Express **27**, 11361–11369 (2019).
[52]H. Hoogland, W. Hänsel, and R. Holzwarth, "Novel robust 2−μm all-PM thulium/holmium based femtosecond fiber laser oscillator," in *Conference on Lasers and Electro-Optics* (Optical Society of America, 2017), p. SM3L.4.
[53]M. Jung, J. Lee, J. Park, J. Koo, Y. M. Jhon, and J. H. Lee, "Mode-locked, 1.94-μm, all-fiberized laser using WS_2 based evanescent field interaction," Opt. Express **23**, 19996–20006 (2015).
[54]H. Yu, X. Zheng, K. Yin, X. Cheng, and T. Jiang, "Thulium/holmium-doped fiber laser passively mode locked by black phosphorus nanoplatelets-based saturable absorber," Appl. Opt. **54**, 10290–10294 (2015).
[55]R. Gumenyuk, M. S. Gaponenko, K. V. Yumashev, A. A. Onushchenko, and O. G. Okhotnikov, "Vector soliton bunching in thulium-holmium fiber laser mode-locked with PbS-quantum-dot-doped glass absorber," IEEE J. Quantum Electron. **48**, 903–907 (2012).
[56]A. E. Akosman and M. Y. Sander, "Low noise, mode-locked 253 MHz Tm/Ho fiber laser with core pumping at 790 nm," IEEE Photonics Technol. Lett. **28**, 1878–1881 (2016).
[57]I. A. Bufetov, M. A. Melkumov, S. V. Firstov, K. E. Riumkin, A. V. Shubin, V. F. Khopin, A. N. Guryanov, and E. M. Dianov, "Bi-doped optical fibers and fiber lasers," IEEE J. Sel. Top. Quantum Electron. **20**, 111–125 (2014).
[58]Y. Fujimoto and M. Nakatsuka, "Infrared luminescence from bismuth-doped silica glass," Jpn. J. Appl. Phys. **40**, L279 (2001).
[59]E. M. Dianov, "Bismuth-doped optical fibers: A challenging active medium for near-IR lasers and optical amplifiers," Light Sci. Appl. **1**, e12–e12 (2012).
[60]A. Khegai, M. Melkumov, K. Riumkin, V. Khopin, S. Firstov, and E. Dianov, "NALM-based bismuth-doped fiber laser at 1.7 μm," Opt. Lett. **43**, 1127–1130 (2018).
[61]T. Noronen, S. Firstov, E. Dianov, and O. G. Okhotnikov, "1700 nm dispersion managed mode-locked bismuth fiber laser," Sci. Rep. **6**, 1–6 (2016).
[62]M. Zhang, E. Kelleher, F. Torrisi, Z. Sun, T. Hasan, D. Popa, F. Wang, A. Ferrari, S. Popov, and J. Taylor, "Tm-doped fiber laser mode-locked by graphene-polymer composite," Opt. Express **20**, 25077–25084 (2012).
[63]E. Anashkina, A. Andrianov, M. Y. Koptev, V. Mashinsky, S. Muravyev, and A. Kim, "Generating tunable optical pulses over the ultrabroad range of 1.6−2.5 μm in GeO_2-doped silica fibers with an Er:fiber laser source," Opt. Express **20**, 27102–27107 (2012).
[64]M. A. Chernysheva, A. A. Krylov, N. R. Arutyunyan, A. S. Pozharov, E. D. Obraztsova, and E. M. Dianov, "SESAM and SWCNT mode-locked all-fiber thulium-doped lasers based on the nonlinear amplifying loop mirror," IEEE J. Sel. Top. Quantum Electron. **20**, 448–455 (2014).
[65]Y. Li, T. Du, B. Xu, H. Xu, Z. Cai, V. M. Mashinsky, and Z. Luo, "Compact all-fiber 2.1−2.7 μm tunable Raman soliton source based on germania-core fiber," Opt. Express **27**, 28544–28550 (2019).
[66]Y. Chen, S. Chen, R. Sidharthan, C. J. Cheng, K. Liu, S. Rao, O. Bang, Q. Wang, D. Tang, and S. Yoo, "High energy ultrafast laser at 2 μm using dispersion engineered thulium-doped fiber," IEEE Photonics J. **11**, 1–12 (2019).
[67]S. Kawakami, S. Nishida, and M. Sumi, "Special issue paper. Transmission characteristics of W-type optical fibres," in *Proceedings of the Institution of Electrical Engineers* (IET, 1976), Vol. 123(6), pp. 586–590.
[68]V. Bhagavatula, M. Spotz, W. Love, and D. Keck, "Segmented-core single-mode fibres with low loss and low dispersion," Electron. Lett. **19**, 317–318 (1983).
[69]S. Chen, Y. Chen, K. Liu, R. Sidharthan, H. Li, C. J. Chang, Q. J. Wang, D. Tang, and S. Yoo, "All-fiber short-wavelength tunable mode-locked fiber laser using normal dispersion thulium-doped fiber," Opt. Express **28**, 17570–17580 (2020).
[70]N. Modsching, P. Kadwani, R. A. Sims, L. Leick, J. Broeng, L. Shah, and M. Richardson, "Lasing in thulium-doped polarizing photonic crystal fiber," Opt. Lett. **36**, 3873–3875 (2011).
[71]F. Stutzki, C. Gaida, M. Gebhardt, F. Jansen, C. Jauregui, J. Limpert, and A. Tünnermann, "Tm-based fiber-laser system with more than 200 MW peak power," Opt. Lett. **40**, 9–12 (2015).
[72]C. Xu and F. Wise, "Recent advances in fibre lasers for nonlinear microscopy," Nat. Photonics **7**, 875–882 (2013).
[73]M. Pang, W. He, and P. S. J. Russell, "Gigahertz-repetition-rate Tm-doped fiber laser passively mode-locked by optoacoustic effects in nanobore photonic crystal fiber," Opt. Lett. **41**, 4601–4604 (2016).
[74]P. Peterka, P. Honzátko, I. Kašík, J. Cajzl, and O. Podrazky, "Thulium-doped optical fibers and components for fiber lasers in 2 μm spectral range," in *Optical Conference on Wave and Quantum Aspects of Contemporary Optics* (International Society for Optics and Photonics, 2014), Vol. 9441, p. 94410B.
[75]J. Cajzl, P. Peterka, M. Kowalczyk, J. Tarka, G. Sobon, J. Sotor, J. Aubrecht, P. Honzátko, and I. Kašík, "Thulium-doped silica fibers with enhanced fluorescence lifetime and their application in ultrafast fiber lasers," Fibers **6**, 66 (2018).
[76]Z. Fang, X. Xiao, X. Wang, Z. Ma, E. Lewis, G. Farrell, P. Wang, J. Ren, H. Guo, and J. Qiu, "Glass-ceramic optical fiber containing $Ba_2TiSi_2O_8$ nanocrystals for frequency conversion of lasers," Sci. Rep. **7**, 44456 (2017).
[77]G. Nemova and R. Kashyap, "Laser cooling with Tm^{3+}-doped oxy-fluoride glass ceramic," J. Opt. Soc. Am. B **29**, 3034–3038 (2012).
[78]L. Cormier and S. Zhou, "Transition metals as optically active dopants in glass-ceramics," Appl. Phys. Lett. **116**, 260503 (2020).
[79]J. R. Sparks, S. C. Aro, R. He, M. L. Goetz, J. P. Krug, S. A. McDaniel, P. A. Berry, G. Cook, K. L. Schepler, P. J. Sazio *et al.*, "Chromium-doped Zinc selenide optical fiber lasers," Opt. Mater. Express **10**, 1843–1852 (2020).
[80]G. Sobon, A. Duzynska, M. Świniarski, J. Judek, J. Sotor, and M. Zdrojek, "CNT-based saturable absorbers with scalable modulation depth for thulium-doped fiber lasers operating at 1.9 μm," Sci. Rep. **7**, 45491 (2017).
[81]Y.-R. Wang, P. Lee, B.-T. Zhang, Y.-H. Sang, J.-L. He, H. Liu, and C.-K. Lee, "Optical nonlinearity engineering of a bismuth telluride saturable absorber and application of a pulsed solid state laser therein," Nanoscale **9**, 19100–19107 (2017).

[82]R. C. Sharp, D. E. Spock, N. Pan, and J. Elliot, "190-fs passively mode-locked thulium fiber laser with a low threshold," Opt. Lett. **21**, 881–883 (1996).
[83]S. Kivisto, T. Hakulinen, M. Guina, and O. G. Okhotnikov, "Tunable raman soliton source using mode-locked Tm-Ho fiber laser," IEEE Photonics Technol. Lett. **19**, 934–936 (2007).
[84]R. Gumenyuk, I. Vartiainen, H. Tuovinen, and O. G. Okhotnikov, "Dissipative dispersion-managed soliton 2 μm thulium/holmium fiber laser," Opt. Lett. **36**, 609–611 (2011).
[85]Q. Wang, J. Geng, Z. Jiang, T. Luo, and S. Jiang, "Mode-locked Tm–Ho-codoped fiber laser at 2.06 μm," IEEE Photonics Technol. Lett. **23**, 682–684 (2011).
[86]U. Keller, K. J. Weingarten, F. X. Kartner, D. Kopf, B. Braun, I. D. Jung, R. Fluck, C. Honninger, N. Matuschek, and J. aus der Au, "Semiconductor saturable absorber mirrors (SESAM's) for femtosecond to nanosecond pulse generation in solid-state lasers," IEEE J. Sel. Top. Quantum Electron. **2**, 435–453 (1996).
[87]BATOP GmbH, see www.batop.de/products/saturable-absorber/saturable-absorber/saturable-absorber_flyer.pdf for "Saturable absorber in transmission: Product overview" (accessed 10 May 2020).
[88]M. J. Lederer, B. Luther-Davies, H. H. Tan, C. Jagadish, M. Haiml, U. Siegner, and U. Keller, "Nonlinear optical absorption and temporal response of arsenic- and oxygen-implanted GaAs," Appl. Phys. Lett. **74**, 1993–1995 (1999).
[89]J. Paajaste, S. Suomalainen, A. Härkönen, U. Griebner, G. Steinmeyer, and M. Guina, "Absorption recovery dynamics in 2 μm GaSb-based SESAMs," J. Phys. D Appl. Phys. **47**, 065102 (2014).
[90]V. Aleksandrov, A. Gluth, V. Petrov, I. Buchvarov, G. Steinmeyer, J. Paajaste, S. Suomalainen, A. Härkönen, M. Guina, X. Mateos, F. Díaz, and U. Griebner, "Mode-locked Tm, Ho:KLu(WO(4))(2) laser at 2060 nm using InGaSb-based SESAMs," Opt. Express **23**, 4614–4619 (2015).
[91]J. Ma, G. Xie, P. Lv, W. Gao, P. Yuan, L. Qian, U. Griebner, V. Petrov, H. Yu, H. Zhang, and J. Wang, "Wavelength-versatile graphene-gold film saturable absorber mirror for ultra-broadband mode-locking of bulk lasers," Sci. Rep. **4**, 5016 (2014).
[92]G. Xing, H. Guo, X. Zhang, T. C. Sum, and C. H. A. Huan, "The physics of ultrafast saturable absorption in graphene," Opt. Express **18**, 4564–4573 (2010).
[93]D. B. S. Soh, R. Hamerly, and H. Mabuchi, "Comprehensive analysis of the optical Kerr coefficient of graphene," Phys. Rev. A **94**, 023845 (2016).
[94]J. L. Cheng, N. Vermeulen, and J. E. Sipe, "Third order optical nonlinearity of graphene," New J. Phys. **16**, 053014 (2014).
[95]Q. Bao, H. Zhang, Z. Ni, Y. Wang, L. Polavarapu, Z. Shen, Q.-H. Xu, D. Tang, and K. P. Loh, "Monolayer graphene as a saturable absorber in a mode-locked laser," Nano Res. **4**, 297–307 (2011).
[96]F. Bonaccorso, Z. Sun, T. Hasan, and A. C. Ferrari, "Graphene photonics and optoelectronics," Nat. Photonics **4**, 611–622 (2010).
[97]G. Sobon, J. Sotor, I. Pasternak, A. Krajewska, W. Strupinski, and K. M. Abramski, "All-polarization maintaining, graphene-based femtosecond Tm-doped all-fiber laser," Opt. Express **23**, 9339–9346 (2015).
[98]Q. Bao, H. Zhang, Y. Wang, Z. Ni, Y. Yan, Z. X. Shen, K. P. Loh, and D. Y. Tang, "Atomic-layer graphene as a saturable absorber for ultrafast pulsed lasers," Adv. Funct. Mater. **19**, 3077–3083 (2009).
[99]S. Yamashita, "Nonlinear optics in carbon nanotube, graphene, and related 2D materials," APL Photonics **4**, 034301 (2019).
[100]M. Pawliszewska, A. Przewloka, and J. Z. Sotor, "Stretched-pulse Ho-doped fiber laser mode-locked by graphene based saturable absorber," in *Fiber Lasers XV: Technology and Systems*, edited by A. L. Carter and I. Hartl (SPIE, 2018), p. 45.
[101]A. Roberts, D. Cormode, C. Reynolds, T. Newhouse-Illige, B. J. LeRoy, and A. S. Sandhu, "Response of graphene to femtosecond high-intensity laser irradiation," Appl. Phys. Lett. **99**, 051912 (2011).
[102]M. Chernysheva, A. Rozhin, Y. Fedotov, C. Mou, R. Arif, S. M. Kobtsev, E. M. Dianov, and S. K. Turitsyn, "Carbon nanotubes for ultrafast fibre lasers," Nanophotonics **6**, 1–30 (2017).
[103]H. Yang, B. Fu, D. Li, Y. Tian, Y. Chen, M. Mattila, Z. Yong, R. Li, A. Hassanien, C. Yang, I. Tittonen, Z. Ren, J. Bai, Q. Li, E. I. Kauppinen, H. Lipsanen, and Z. Sun, "Broadband laser polarization control with aligned carbon nanotubes," Nanoscale **7**, 11199–11205 (2015).
[104]Y. Tian, A. G. Nasibulin, B. Aitchison, T. Nikitin, J. V. Pfaler, H. Jiang, Z. Zhu, L. Khriachtchev, D. P. Brown, and E. I. Kauppinen, "Controlled synthesis of single-walled carbon nanotubes in an aerosol reactor," J. Phys. Chem. C **115**, 7309–7318 (2011).
[105]Y. Gladush, A. A. Mkrtchyan, D. S. Kopylova, A. Ivanenko, B. Nyushkov, S. Kobtsev, A. Kokhanovskiy, A. Khegai, M. Melkumov, M. Burdanova *et al.*, "Ionic liquid gated carbon nanotube saturable absorber for switchable pulse generation," Nano Lett. **19**, 5836–5843 (2019).
[106]T. Hasan, Z. Sun, P. Tan, D. Popa, E. Flahaut, E. J. R. Kelleher, F. Bonaccorso, F. Wang, Z. Jiang, F. Torrisi, G. Privitera, V. Nicolosi, and A. C. Ferrari, "Double-wall carbon nanotubes for wide-band, ultrafast pulse generation," ACS Nano **8**, 4836–4847 (2014).
[107]M. Chernysheva, A. Bednyakova, M. Al Araimi, R. C. T. Howe, G. Hu, T. Hasan, A. Gambetta, G. Galzerano, M. Rümmeli, and A. Rozhin, "Double-wall carbon nanotube hybrid mode-locker in Tm-doped fibre laser: A novel mechanism for robust bound-state solitons generation," Sci. Rep. **7**, 44314 (2017).
[108]H. Hirori, K. Matsuda, and Y. Kanemitsu, "Exciton energy transfer between the inner and outer tubes in double-walled carbon nanotubes," Phys. Rev. B **78**, 113409 (2008).
[109]Y. Cui and X. Liu, "Graphene and nanotube mode-locked fiber laser emitting dissipative and conventional solitons," Opt. Express **21**, 18969–18974 (2013).
[110]V. Tran, R. Soklaski, Y. Liang, and L. Yang, "Layer-controlled band gap and anisotropic excitons in few-layer black phosphorus," Phys. Rev. B **89**, 235319 (2014).
[111]D. Li, H. Jussila, L. Karvonen, G. Ye, H. Lipsanen, X. Chen, and Z. Sun, "Polarization and thickness dependent absorption properties of black phosphorus: New saturable absorber for ultrafast pulse generation," Sci. Rep. **5**, 15899 (2015).
[112]H. Yuan, X. Liu, F. Afshinmanesh, W. Li, G. Xu, J. Sun, B. Lian, A. G. Curto, G. Ye, Y. Hikita, Z. Shen, S.-C. Zhang, X. Chen, M. Brongersma, H. Y. Hwang, and Y. Cui, "Polarization-sensitive broadband photodetector using a black phosphorus vertical p-n junction," Nat. Nanotechnol. **10**, 707–713 (2015).
[113]J. Sotor, G. Sobon, M. Kowalczyk, W. Macherzynski, P. Paletko, and K. M. Abramski, "Ultrafast thulium-doped fiber laser mode locked with black phosphorus," Opt. Lett. **40**, 3885–3888 (2015).
[114]D. Na, K. Park, K.-H. Park, and Y.-W. Song, "Passivation of black phosphorus saturable absorbers for reliable pulse formation of fiber lasers," Nanotechnology **28**, 475207 (2017).
[115]X. Jin, G. Hu, M. Zhang, T. Albrow-Owen, Z. Zheng, and T. Hasan, "Environmentally stable black phosphorus saturable absorber for ultrafast laser," Nanophotonics **9**, 2445–2449 (2020).
[116]M. Batmunkh, M. Bat-Erdene, and J. G. Shapter, "Black phosphorus: Synthesis and application for solar cells," Adv. Energy Mater. **8**, 1701832 (2018).
[117]G. Hu, T. Albrow-Owen, X. Jin, A. Ali, Y. Hu, R. C. Howe, K. Shehzad, Z. Yang, X. Zhu, R. I. Woodward *et al.*, "Black phosphorus ink formulation for inkjet printing of optoelectronics and photonics," Nat. Commun. **8**, 1–10 (2017).
[118]Z. Guo, H. Zhang, S. Lu, Z. Wang, S. Tang, J. Shao, Z. Sun, H. Xie, H. Wang, X.-F. Yu, and P. K. Chu, "From black phosphorus to phosphorene: Basic solvent exfoliation, evolution of Raman scattering, and applications to ultrafast photonics," Adv. Funct. Mater. **25**, 6996–7002 (2015).
[119]C. Zhao, Y. Zou, Y. Chen, Z. Wang, S. Lu, H. Zhang, S. Wen, and D. Tang, "Wavelength-tunable picosecond soliton fiber laser with topological insulator: Bi_2Se_3 as a mode locker," Opt. Express **20**, 27888–27895 (2012).
[120]J.-L. Xu, Y.-J. Sun, J.-L. He, Y. Wang, Z.-J. Zhu, Z.-Y. You, J.-F. Li, M. M. C. Chou, C.-K. Lee, and C.-Y. Tu, "Ultrasensitive nonlinear absorption response of large-size topological insulator and application in low-threshold bulk pulsed lasers," Sci. Rep. **5**, 14856 (2015).
[121]J. Zhao, Z. Xu, Y. Zang, Y. Gong, X. Zheng, K. He, X. Cheng, and T. Jiang, "Thickness-dependent carrier and phonon dynamics of topological insulator Bi^2Te^3 thin films," Opt. Express **25**, 14635–14643 (2017).

[122]H. Zhang, C.-X. Liu, X.-L. Qi, X. Dai, Z. Fang, and S.-C. Zhang, "Topological insulators in Bi_2Se_3, Bi_2Te_3 and Sb_2Te_3 with a single dirac cone on the surface," Nat. Phys. **5**, 438–442 (2009).
[123]R. Miao, Y. Hu, and J. Tian, "Control of saturable absorption of topological insulator Bi_2Se_3 by electron and hole doping," in *National Conference on Laser Technology and Optoelectronics* (SPIE, 2019), p. 81.
[124]J. Wang, J. Yin, T. He, and P. Yan, "Sb_2Te_3 mode-locked ultrafast fiber laser at 1.93 μm," Chin. Phys. B **27**, 084214 (2018).
[125]J. Lee, Y. Kim, and J. H. Lee, "Femtosecond Tm-Ho co-doped fiber laser using a CoSb 3-Skutterudite-based passive mode-locker," in *Conference on Lasers and Electro-Optics Europe* (IEEE, 2019), pp. CF–P–58.
[126]M. Jung, J. Lee, J. Koo, J. Park, Y.-W. Song, K. Lee, S. Lee, and J. H. Lee, "A femtosecond pulse fiber laser at 1935 nm using a bulk-structured Bi_2Te_3 topological insulator," Opt. Express **22**, 7865–7874 (2014).
[127]K. F. Mak, C. Lee, J. Hone, J. Shan, and T. F. Heinz, "Atomically thin MoS_2: A new direct-gap semiconductor," Phys. Rev. Lett. **105**, 136805 (2010).
[128]Z. Tian, K. Wu, L. Kong, N. Yang, Y. Wang, R. Chen, W. Hu, J. Xu, and Y. Tang, "Mode-locked thulium fiber laser with MoS_2," Laser Phys. Lett. **12**, 065104 (2015).
[129]X. Jiang, S. Liu, W. Liang, S. Luo, Z. He, Y. Ge, H. Wang, R. Cao, F. Zhang, Q. Wen, J. Li, Q. Bao, D. Fan, and H. Zhang, "Broadband nonlinear photonics in few-layer MXene $Ti_3C_2T_x$ (T = F, O, or OH)," Laser Photonics Rev. **12**, 1700229 (2018).
[130]Y. Dong, S. Chertopalov, K. Maleski, B. Anasori, L. Hu, S. Bhattacharya, A. M. Rao, Y. Gogotsi, V. N. Mochalin, and R. Podila, "Saturable absorption in 2D Ti_3C_2 MXene thin films for passive photonic diodes," Adv. Mater. **30**, 1705714 (2018).
[131]M. Seredych, C. E. Shuck, D. Pinto, M. Alhabeb, E. Precetti, G. Deysher, B. Anasori, N. Kurra, and Y. Gogotsi, "High-temperature behavior and surface chemistry of carbide MXenes studied by thermal analysis," Chem. Mater. **31**, 3324–3332 (2019).
[132]Z. Wang, H. Li, M. Luo, T. Chen, X. Xia, H. Chen, C. Ma, J. Guo, Z. He, Y. Song, J. Liu, X. Jiang, and H. Zhang, "MXene photonic devices for near-infrared to mid-infrared ultrashort pulse generation," ACS Appl. Nano Mater. **3**, 3513–3522 (2020).
[133]Y. Shang, J. Wen, Y. Dong, H. Zhan, Y. Luo, G.-D. Peng, X. Zhang, F. Pang, Z. Chen, and T. Wang, "Luminescence properties of PbS quantum-dot-doped silica optical fibre produced via atomic layer deposition," J. Lumin. **187**, 201–204 (2017).
[134]M. Chernysheva, M. A. Araimi, G. A. Rance, N. J. Weston, B. Shi, S. Saied, J. L. Sullivan, N. Marsh, and A. Rozhin, "Revealing the nature of morphological changes in carbon nanotube-polymer saturable absorber under high-power laser irradiation," Sci. Rep. **8**, 7491 (2018).
[135]H.-J. Kim, H.-J. Choi, S.-M. Nam, and Y.-W. Song, "High-performance laser mode-locker with glass-hosted SWNTs realized by room-temperature aerosol deposition," Opt. Express **19**, 4762–4767 (2011).
[136]P. Loiko, J. M. Serres, S. S. Delekta, E. Kifle, J. Bogusławski, M. Kowalczyk, J. Sotor, M. Aguiló, F. Díaz, U. Griebner, V. Petrov, S. Popov, J. Li, X. Mateos, and M. Östling, "Inkjet-printing of graphene saturable absorbers for ~2 μm bulk and waveguide lasers," Opt. Mater. Express **8**, 2803 (2018).
[137]X. Jiang, W. Li, T. Hai, R. Yue, Z. Chen, C. Lao, Y. Ge, G. Xie, Q. Wen, and H. Zhang, "Inkjet-printed MXene micro-scale devices for integrated broadband ultrafast photonics," NPJ 2D Mater. Appl. **3**, 1–9 (2019).
[138]Y. Song, Z. Liang, X. Jiang, Y. Chen, Z. Li, L. Lu, Y. Ge, K. Wang, J. Zheng, S. Lu, J. Ji, and H. Zhang, "Few-layer antimonene decorated microfiber: Ultra-short pulse generation and all-optical thresholding with enhanced long term stability," 2D Mater. **4**, 045010 (2017).
[139]T. Chai, X. Li, T. Feng, P. Guo, Y. Song, Y. Chen, and H. Zhang, "Few-layer bismuthene for ultrashort pulse generation in a dissipative system based on an evanescent field," Nanoscale **10**, 17617–17622 (2018).
[140]X. Zhu, F. Li, Y. Wang, M. Qiao, and Y. Li, "Pd_2Se_3 monolayer: A novel two-dimensional material with excellent electronic, transport, and optical properties," J. Mater. Chem. C **6**, 4494–4500 (2018).
[141]M. Fan, T. Li, G. Li, H. Ma, S. Zhao, K. Yang, and C. Kränkel, "Graphitic C_3N_4 as a new saturable absorber for the mid-infrared spectral range," Opt. Lett. **42**, 286–289 (2017).
[142]B. Janaszek, A. Tyszka-Zawadzka, and P. Szczepański, "Control of gain/absorption in tunable hyperbolic metamaterials," Opt. Express **25**, 13153–13162 (2017).
[143]J. Guo, Z. Wang, R. Shi, Y. Zhang, Z. He, L. Gao, R. Wang, Y. Shu, C. Ma, Y. Ge *et al.*, "Graphdiyne as a promising mid-infrared nonlinear optical material for ultrafast photonics," Adv. Opt. Mater. **8**, 2000067 (2020).
[144]J. Guo, R. Shi, R. Wang, Y. Wang, F. Zhang, C. Wang, H. Chen, C. Ma, Z. Wang, Y. Ge *et al.*, "Graphdiyne-polymer nanocomposite as a broadband and robust saturable absorber for ultrafast photonics," Laser Photonics Rev. **14**, 1900367 (2020).
[145]J. Wang, A. Coillet, O. Demichel, Z. Wang, D. Rego, A. Bouhelier, P. Grelu, and B. Cluzel, "Saturable plasmonic metasurfaces for laser mode locking," Light Sci. Appl. **9**, 1–9 (2020).
[146]Z. Kang, M. Liu, X. Gao, N. Li, S. Yin, G. Qin, and W. Qin, "Mode-locked thulium-doped fiber laser at 1982 nm by using a gold nanorods saturable absorber," Laser Phys. Lett. **12**, 045105 (2015).
[147]H. Huang, M. Li, P. Liu, L. Jin, H. Wang, and D. Shen, "Gold nanorods as the saturable absorber for a diode-pumped nanosecond q-switched 2 μm solid-state laser," Opt. Lett. **41**, 2700–2703 (2016).
[148]V. Voropaev, A. Donodin, A. Voronets, V. Lazarev, M. Tarabrin, V. Karasik, and A. Krylov, "High-power passively mode-locked thulium-doped all-fiber ring laser with nonlinearity and dispersion management," in *2018 International Conference Laser Optics (ICLO)* (IEEE, 2018), pp. 18–18.
[149]B. Sun, J. Luo, B. P. Ng, and X. Yu, "Dispersion-compensation-free femtosecond Tm-doped all-fiber laser with a 248 MHz repetition rate," Opt. Lett. **41**, 4052–4055 (2016).
[150]K. Özgören and F. Ö. İlday, "All-fiber all-normal dispersion laser with a fiber-based Lyot filter," Opt. Lett. **35**, 1296–1298 (2010).
[151]N. Kanagaraj, A. Theodosiou, J. Aubrecht, P. Peterka, M. Kamradek, K. Kalli, I. Kasik, and P. Honzatko, "All-fiber mode-locked thulium-doped fiber laser using a novel femtosecond-laser-inscribed 45°-plane-by-plane-tilted fiber grating," Laser Phys. Lett. **16**, 095104 (2019).
[152]Z. Yan, C. Mou, H. Wang, K. Zhou, Y. Wang, W. Zhao, and L. Zhang, "All-fiber polarization interference filters based on 45°-tilted fiber gratings," Opt. Lett. **37**, 353–355 (2012).
[153]V. I. Kopp, V. M. Churikov, J. Singer, N. Chao, D. Neugroschl, and A. Z. Genack, "Chiral fiber gratings," Science **305**, 74–75 (2004).
[154]Y. Du, X. Shu, and Z. Xu, "All-fiber passively mode-locked laser based on a chiral fiber grating," Opt. Lett. **41**, 360–363 (2016).
[155]R. A. Bergh, H. C. Lefevre, and H. J. Shaw, "Single-mode fiber-optic polarizer," Opt. Lett. **5**, 479–481 (1980).
[156]G. Li and A. Xu, "Analysis of the TE-pass or TM-pass metal-clad polarizer with a resonant buffer layer," J. Lightwave Technol. **26**, 1234–1241 (2008).
[157]H. Jiang, Y. Huang, Z. Zhao, L. Jin, S. Yamashita, and S. Y. Set, "Passively mode-locked thulium-doped all-fiber laser based on low V number fiber bending," arXiv preprint arXiv:2001.01386 (2020).
[158]N. Doran and D. Wood, "Nonlinear-optical loop mirror," Opt. Lett. **13**, 56–58 (1988).
[159]M. E. Fermann, F. Haberl, M. Hofer, and H. Hochreiter, "Nonlinear amplifying loop mirror," Opt. Lett. **15**, 752–754 (1990).
[160]A. Steele, "Pulse compression by an optical fibre loop mirror constructed from two different fibres," Electron. Lett. **29**, 1972–1974 (1993).
[161]W. S. Wong, S. Namiki, M. Margalit, H. A. Haus, and E. P. Ippen, "Self-switching of optical pulses in dispersion-imbalanced nonlinear loop mirrors," Opt. Lett. **22**, 1150–1152 (1997).
[162]K. Smith, N. Doran, and P. Wigley, "Pulse shaping, compression, and pedestal suppression employing a nonlinear-optical loop mirror," Opt. Lett. **15**, 1294–1296 (1990).
[163]J. Li, Z. Zhang, Z. Sun, H. Luo, Y. Liu, Z. Yan, C. Mou, L. Zhang, and S. K. Turitsyn, "All-fiber passively mode-locked Tm-doped NOLM-based

oscillator operating at 2-μm in both soliton and noisy-pulse regimes," Opt. Express **22**, 7875–7882 (2014).
[164]X. Wang, X. Peng, and J. Zhang, "Multistate passively mode-locked thulium-doped fiber laser with nonlinear amplifying loop mirror," Appl. Opt. **57**, 3410–3414 (2018).
[165]H. Yulian, L. Hongyu, L. Jing, L. Zhuo, and L. Jianfeng, "High power all-fiber passively mode-locked thulium-doped fiber laser," High Power Laser Part. Beams **26**, 26101013 (2014).
[166]M. Michalska and J. Swiderski, "All-fiber thulium-doped mode-locked fiber laser and amplifier based on nonlinear fiber loop mirror," Opt. Laser Technol. **118**, 121–125 (2019).
[167]J. Zhao, J. Zhou, Y. Jiang, L. Li, D. Shen, A. Komarov, L. Su, D. Tang, M. Klimczak, and Z. Luming, "Nonlinear absorbing-loop mirror in a holmium-doped fiber laser," J. Lightwave Technol. **38**, 6069–6075 (2020).
[168]M. Chernysheva, C. Mou, R. Arif, M. AlAraimi, M. Rümmeli, S. Turitsyn, and A. Rozhin, "High power Q-switched thulium-doped fibre laser using carbon nanotube polymer composite saturable absorber," Sci. Rep. **6**, 24220 (2016).
[169]Y. Lyu, J. Li, Y. Hu, Y. Wang, C. Wei, and Y. Liu, "Theoretical comparison of NPR and hybrid mode-locked soliton thulium-doped fiber lasers," IEEE Photonics J. **9**, 1–11 (2017).
[170]F. Haxsen, D. Wandt, U. Morgner, J. Neumann, and D. Kracht, "Hybrid mode-locked thulium soliton fiber laser," in *IEEE Photonic Society 24th Annual Meeting* (IEEE, 2011), pp. 885–886.
[171]M. A. Chernysheva, A. A. Krylov, N. R. Arutyunyan, A. S. Pozharov, E. D. Obraztsova, and E. M. Dianov, "Sesam and SWCNT mode-locked all-fiber thulium-doped lasers based on the nonlinear amplifying loop mirror," IEEE J. Sel. Top. Quantum Electron. **20**, 448–455 (2014).
[172]S. D. Lim, J. Gene, S. K. Kim, and D. il Yeom, "Hybrid mode-locked 2 μm fiber laser with sub-megahertz repetition rate," in *Conference on Lasers and Electro-Optics* (Optical Society of America, 2018), p. SM2N.5.
[173]H. Li, F. Hu, C. Li, Y. Tian, C. Huang, J. Zhang, and S. Xu, "Generation of switchable multiwavelength solitons with wide wavelength spacing at 2 μm," Opt. Lett. **44**, 2442–2445 (2019).
[174]S. A. Filatova, V. A. Kamynin, N. R. Arutyunyan, A. S. Pozharov, A. I. Trikshev, I. V. Zhluktova, I. O. Zolotovskii, E. D. Obraztsova, and V. B. Tsvetkov, "Hybrid mode locking of an all-fiber holmium laser," J. Opt. Soc. Am. B **35**, 3122–3125 (2018).
[175]E. Nazemosadat and A. Mafi, "Nonlinear multimodal interference and saturable absorption using a short graded-index multimode optical fiber," J. Opt. Soc. Am. B **30**, 1357–1367 (2013).
[176]H. Li, Z. Wang, C. Li, J. Zhang, and S. Xu, "Mode-locked Tm fiber laser using SMF-SIMF-GIMF-SMF fiber structure as a saturable absorber," Opt. Express **25**, 26546–26553 (2017).
[177]G. J. Liu, B. M. Liang, Q. Li, and G. L. Jin, "Beam propagation in nonlinear multimode interference waveguide," J. Opt. A: Pure Appl. Opt. **7**, 457–462 (2005).
[178]A. S. Karar, T. Smy, and A. L. Steele, "Nonlinear dynamics of a passively mode-locked fiber laser containing a long-period fiber grating," IEEE J. Quantum Electron. **44**, 254–261 (2008).
[179]T. F. Büttner, D. D. Hudson, E. C. Mägi, A. C. Bedoya, T. Taunay, and B. J. Eggleton, "Multicore, tapered optical fiber for nonlinear pulse reshaping and saturable absorption," Opt. Lett. **37**, 2469–2471 (2012).
[180]H. Jiang, H. Li, F. Hu, X. Ren, C. Li, and S. Xu, "Mode-locked Tm fiber laser with a tapered GIMF SA based on nonlinear multimode interference effect," IEEE Photonics Technol. Lett. **32**, 503–506 (2020).
[181]H. Zhang, L. Jin, H. Zhang, Y. Xu, L. Shi, T. Wang, H. Chen, D. Wang *et al.*, "All-fiber nonlinear optical switch based on polarization controller coiled SMF–GIMF–SMF for ultrashort pulse generation," Opt. Commun. **452**, 7–11 (2019).
[182]Z. Wang, D. Wang, F. Yang, L. Li, C. Zhao, B. Xu, S. Jin, S. Cao, and Z. Fang, "Er-doped mode-locked fiber laser with a hybrid structure of a step-index–graded-index multimode fiber as the saturable absorber," J. Lightwave Technol. **35**, 5280–5285 (2017).
[183]K. Zhao, Y. Li, X. Xiao, and C. Yang, "Nonlinear multimode interference-based dual-color mode-locked fiber laser," Opt. Lett. **45**, 1655–1658 (2020).
[184]K. Regelskis, J. Želudevičius, K. Viskontas, and G. Račiukaitis, "Ytterbium-doped fiber ultrashort pulse generator based on self-phase modulation and alternating spectral filtering," Opt. Lett. **40**, 5255–5258 (2015).
[185]P. Wang, S. Yao, P. Grelu, X. Xiao, and C. Yang, "Pattern formation in 2-μm Tm Mamyshev oscillators associated with the dissipative faraday instability," Photonics Res. **7**, 1287–1295 (2019).
[186]P. Repgen, B. Schuhbauer, M. Hinkelmann, D. Wandt, A. Wienke, U. Morgner, J. Neumann, and D. Kracht, "Mode-locked pulses from a thulium-doped fiber Mamyshev oscillator," Opt. Express **28**, 13837–13844 (2020).
[187]R. Dai, Y. Meng, Y. Li, J. Qin, S. Zhu, and F. Wang, "Nanotube mode-locked, wavelength and pulsewidth tunable thulium fiber laser," Opt. Express **27**, 3518–3527 (2019).
[188]T. Qiao, H. Cheng, X. Wen, W. Wang, W. Lin, Y. Zhou, Y. Guo, Y. Liu, and Z. Yang, "High-power 2 GHz fs pulsed all-fiber amplified laser system at 2.0 μm," Opt. Lett. **44**, 6001–6004 (2019).
[189]D. Gaponov, L. Lavoute, N. Ducros, A. Hideur, and S. Février, "10 μJ-class compact thulium all-fibered CPA system," in *The European Conference on Lasers and Electro-Optics* (Optical Society of America, 2017), p. CJ_11_3.
[190]G. P. Agrawal, *Applications of Nonlinear Fiber Optics* (Elsevier, 2001).
[191]F. Haxsen, D. Wandt, U. Morgner, J. Neumann, and D. Kracht, "Pulse characteristics of a passively mode-locked thulium fiber laser with positive and negative cavity dispersion," Opt. Express **18**, 18981–18988 (2010).
[192]B. Sun, J. Luo, Y. Zhang, Q. Wang, and X. Yu, "65-fs pulses at 2 μm in a compact Tm-doped all-fiber laser by dispersion and nonlinearity management," IEEE Photonics Technol. Lett. **30**, 303–306 (2017).
[193]J. Jiang, C. Mohr, J. Bethge, A. Mills, W. Mefford, I. Hartl, M. E. Fermann, C.-C. Lee, S. Suzuki, T. R. Schibli *et al.*, "500 MHz, 58 fs highly coherent Tm fiber soliton laser," in *CLEO: Science and Innovations* (Optical Society of America, 2012), pp. CTh5D–7.
[194]L. Liu, X. Li, S. Zhang, J. Liu, L. Chen, C. Wang, Y. Xin, Z. Guo, and Z. Yang, "Optimal design of high energy similariton thulium-doped fiber lasers," in *2019 IEEE 4th Optoelectronics Global Conference (OGC)* (IEEE, 2019), pp. 19–22.
[195]Y. Tang, A. Chong, and F. W. Wise, "Generation of 8 nJ pulses from a normal-dispersion thulium fiber laser," Opt. Lett. **40**, 2361–2364 (2015).
[196]N. Yang, C. Huang, Y. Tang, and J. Xu, "12 nJ 2 μm dissipative soliton fiber laser," Laser Phys. Lett. **12**, 055101 (2015).
[197]C. Huang, C. Wang, W. Shang, N. Yang, Y. Tang, and J. Xu, "Developing high energy dissipative soliton fiber lasers at 2 micron," Sci. Rep. **5**, 13680 (2015).
[198]D. Gaponov, R. Dauliat, D. Darwich, T. Mansuryan, R. Jamier, S. Grimm, K. Schuster, and P. Roy, "High-power passively mode-locked dissipative soliton fiber laser featuring cladding-pumped non-CVD thulium-doped fiber," J. Opt. Soc. Am. B **32**, 1656–1659 (2015).
[199]G. Sobon, J. Sotor, T. Martynkien, and K. M. Abramski, "Ultra-broadband dissipative soliton and noise-like pulse generation from a normal dispersion mode-locked Tm-doped all-fiber laser," Opt. Express **24**, 6156–6161 (2016).
[200]J. Wang, X. Liang, G. Hu, Z. Zheng, S. Lin, D. Ouyang, X. Wu, P. Yan, S. Ruan, Z. Sun, and T. Hasan, "152 fs nanotube-mode-locked thulium-doped all-fiber laser," Sci. Rep. **6**, 28885 (2016).
[201]Y. Li, L. Wang, Y. Kang, X. Guo, and L. Tong, "Microfiber-enabled dissipative soliton fiber laser at 2 μm," Opt. Lett. **43**, 6105–6108 (2018).
[202]L.-M. Yang, P. Wan, V. Protopopov, and J. Liu, "2 μm femtosecond fiber laser at low repetition rate and high pulse energy," Opt. Express **20**, 5683–5688 (2012).
[203]Z. Dou, B. Zhang, X. He, Z. Xu, and J. Hou, "High-power and large-energy dissipative soliton resonance in a compact Tm-doped all-fiber laser," IEEE Photonics Technol. Lett. **31**, 381–384 (2019).
[204]B. Ibarra-Escamilla, M. Durán-Sánchez, B. Posada-Ramírez, H. Santiago-Hernández, R. I. Álvarez-Tamayo, D. S. de la Llave, M. Bello-Jiménez, and E. A. Kuzin, "Dissipative soliton resonance in a thulium-doped all-fiber laser operating at large anomalous dispersion regime," IEEE Photonics J. **10**, 1–7 (2018).

[205]S. Liu, F.-P. Yan, L.-N. Zhang, W.-G. Han, Z.-Y. Bai, and H. Zhou, "Noise-like femtosecond pulse in passively mode-locked Tm-doped NALM-based oscillator with small net anomalous dispersion," J. Opt. **18**, 015508 (2015).
[206]G. Sobon, J. Sotor, A. Przewolka, I. Pasternak, W. Strupinski, and K. Abramski, "Amplification of noise-like pulses generated from a graphene-based Tm-doped all-fiber laser," Opt. Express **24**, 20359–20364 (2016).
[207]P. Wang, C. Bao, B. Fu, X. Xiao, P. Grelu, and C. Yang, "Generation of wavelength-tunable soliton molecules in a 2-μm ultrafast all-fiber laser based on nonlinear polarization evolution," Opt. Lett. **41**, 2254–2257 (2016).
[208]K. Yin, B. Zhang, L. Li, T. Jiang, X. Zhou, and J. Hou, "Soliton mode-locked fiber laser based on topological insulator Bi_2Te_3 nanosheets at 2 μm," Photonics Res. **3**, 72–76 (2015).
[209]J. Zhao, L. Li, L. Zhao, D. Tang, D. Shen, and L. Su, "Tunable and switchable harmonic h-shaped pulse generation in a 3.03 km ultralong mode-locked thulium-doped fiber laser," Photonics Res. **7**, 332–340 (2019).
[210]J. Zeng, A. E. Akosman, and M. Y. Sander, "Scaling the repetition rate of thulium-doped ultrafast soliton fiber lasers to the GHz regime," Opt. Express **26**, 24687–24694 (2018).
[211]A. Y. Chamorovskiy, A. Marakulin, A. Kurkov, and O. Okhotnikov, "Tunable Ho-doped soliton fiber laser mode-locked by carbon nanotube saturable absorber," Laser Phys. Lett. **9**, 602 (2012).
[212]R. Liao, Y. Song, W. Liu, H. Shi, L. Chai, and M. Hu, "Dual-comb spectroscopy with a single free-running thulium-doped fiber laser," Opt. Express **26**, 11046–11054 (2018).
[213]J. Olson, Y. Ou, A. Azarm, and K. Kieu, "Bi-directional mode-locked thulium fiber laser as a single-cavity dual-comb source," IEEE Photonics Technol. Lett. **30**, 1772–1775 (2018).
[214]S. Xing, A. S. Kowligy, D. M. Lesko, A. J. Lind, and S. A. Diddams, "All-fiber frequency comb at 2 μm providing 1.4-cycle pulses," Opt. Lett. **45**, 2660–2663 (2020).
[215]M. Gebhardt, C. Gaida, T. Heuermann, F. Stutzki, C. Jauregui, J. Antonio-Lopez, A. Schulzgen, R. Amezcua-Correa, J. Limpert, and A. Tünnermann, "Nonlinear pulse compression to 43 W GW-class few-cycle pulses at 2 μm wavelength," Opt. Lett. **42**, 4179–4182 (2017).
[216]M. Gebhardt, C. Gaida, T. Heuermann, C. Jauregui, J. Antonio-Lopez, A. Schulzgen, R. Amezcua-Correa, J. Rothhardt, and J. Limpert, "Tm:fiber CPA driven nonlinear pulse compression stage delivering multi-GW, sub-10 fs pulses at 20 W of average power," in *Fiber Lasers XVI: Technology and Systems* (International Society for Optics and Photonics, 2019), Vol. 10897, p. 108971E.
[217]C. Gaida, M. Gebhardt, F. Stutzki, C. Jauregui, J. Limpert, and A. Tünnermann, "Self-compression in a solid fiber to 24 MW peak power with few-cycle pulses at 2 μm wavelength," Opt. Lett. **40**, 5160–5163 (2015).
[218]T. Heuermann, C. Gaida, M. Gebhardt, and J. Limpert, "Thulium-doped nonlinear fiber amplifier delivering 50 fs pulses at 20 W of average power," Opt. Lett. **43**, 4441–4444 (2018).
[219]H. Ren, L. Shen, A. F. Runge, T. W. Hawkins, J. Ballato, U. Gibson, and A. C. Peacock, "Low-loss silicon core fibre platform for mid-infrared nonlinear photonics," Light Sci. Appl. **8**, 1–10 (2019).
[220]H. Zia, N. M. Lüpken, T. Hellwig, C. Fallnich, and K.-J. Boller, "Supercontinuum generation in media with sign-alternated dispersion," Laser Photonics Rev. **14**(7), 2000031 (2019).
[221]A. Medjouri and D. Abed, "Design and modelling of all-normal dispersion $As_{39}Se_{61}$ chalcogenide photonic crystal fiber for flat-top coherent mid-infrared supercontinuum generation," Opt. Fiber Technol. **50**, 154–164 (2019).
[222]G. Y. Jiang, Y. J. Fu, Y. Huang, and H. T. Chen, "Generation of the self-similar parabolic pulses by designing comb-like profiled dispersion fiber based on alternately arranged single-mode fibers and dispersion-shifted fibers," Optik **124**, 5328–5331 (2013).
[223]B. Sun, J. Luo, Z. Yan, K. Liu, J. Ji, Y. Zhang, Q. J. Wang, and X. Yu, "1867–2010 nm tunable femtosecond thulium-doped all-fiber laser," Opt. Express **25**, 8997–9002 (2017).
[224]O. Puncken, D. C. Kirsch, A. Wienke, D. Wandt, J. Neumann, and D. Kracht, "Ultrafast thulium fiber laser operating at 1750 nm," in *Conference on Lasers and Electro-Optics Europe* (IEEE, 2017), pp. CJ–13.
[225]C. Li, X. Wei, C. Kong, S. Tan, N. Chen, J. Kang, and K. K. Wong, "Fiber chirped pulse amplification of a short wavelength mode-locked thulium-doped fiber laser," APL Photonics **2**, 121302 (2017).
[226]T. Noronen, O. Okhotnikov, and R. Gumenyuk, "Electronically tunable thulium-holmium mode-locked fiber laser for the 1700–1800 nm wavelength band," Opt. Express **24**, 14703–14708 (2016).
[227]Y. Nomura and T. Fuji, "Ultrafast thulium-doped fiber laser system at 1.8 μm for multiphoton microscopy," in *2019 Conference on Lasers and Electro-Optics (CLEO)* (IEEE, 2019), pp. 1–2.
[228]C. Jauregui, C. Stihler, and J. Limpert, "Transverse mode instability," Adv. Opt. Photonics **12**, 429–484 (2020).
[229]A. V. Smith and J. J. Smith, "Mode instability thresholds for Tm-doped fiber amplifiers pumped at 790 nm," Opt. Express **24**, 975–992 (2016).
[230]C. Gaida, M. Gebhardt, T. Heuermann, Z. Wang, F. Stutzki, C. Jauregui, and J. Limpert, "Observation of transverse-mode instabilities in a thulium-doped fiber amplifier," in *Fiber Lasers XVI: Technology and Systems* (International Society for Optics and Photonics, 2019), Vol. 10897, p. 1089702.
[231]X. Liu, F. Li, X. Yu, S. Zhang, and Y. Tang, "High-pulse-energy mode-locked and Q-switched large-mode-area thulium fiber laser," Opt. Commun. **457**, 124730 (2020).
[232]R. Herda and A. Zach, "All-fiber generation of few-cycle pulses at 1950 nm by triple-stage compression of a thulium-doped laser system," in *2013 IEEE Photonics Conference* (IEEE, 2013), pp. 621–622.
[233]D. Gaponov, L. Lavoute, N. Ducros, M. Paris, A. Hideur, and S. Février, "Compact thulium FCPA system delivering 11 Mw, 530 fs pulses," in *The European Conference on Lasers and Electro-Optics* (Optical Society of America, 2019), p. cj_10_5.
[234]P. Wan, L.-M. Yang, and J. Liu, "156 micro-J ultrafast thulium-doped fiber laser," in *Fiber Lasers X: Technology, Systems, and Applications* (International Society for Optics and Photonics, 2013), Vol. 8601, p. 860138.
[235]C. Gaida, M. Gebhardt, T. Heuermann, Z. Wang, F. Stutzki, C. Jauregui, and J. Limpert, "Ultrafast Tm-doped fiber amplifier with 1 kW average output power," in *The European Conference on Lasers and Electro-Optics* (Optical Society of America, 2019), p. cj_10_4.
[236]Z. Wang, T. Heuermann, M. Gebhardt, C. Gaida, C. Jauregui, and J. Limpert, "108 W average power ultrashort pulses with GW-level peak power from a Tm-doped fiber CPA system," in *Fiber Lasers XVII: Technology and Systems* (International Society for Optics and Photonics, 2020), Vol. 11260, p. 112600K.
[237]M. Gebhardt, C. Gaida, F. Stutzki, R. Klas, M. Tschernajew, S. Demmler, C. Jauregui, J. Rothhardt, J. Limpert, and A. Tünnermann, "Multi-GW, 100 fs thulium-doped fiber laser system for high-harmonic generation at high repetition rates," in *The European Conference on Lasers and Electro-Optics* (Optical Society of America, 2017), p. CJ_11_1.
[238]A. Klenke, M. Müller, H. Stark, F. Stutzki, C. Hupel, T. Schreiber, A. Tünnermann, and J. Limpert, "Coherently combined 16-channel multicore fiber laser system," Opt. Lett. **43**, 1519–1522 (2018).
[239]F. B. Slimen, S. Chen, J. Lousteau, Y. Jung, N. White, S. Alam, D. J. Richardson, and F. Poletti, "Highly efficient Tm^3+ doped germanate large mode area single mode fiber laser," Opt. Mater. Express **9**, 4115–4125 (2019).
[240]F. Poletti, X. Feng, G. M. Ponzo, M. N. Petrovich, W. H. Loh, and D. J. Richardson, "All-solid highly nonlinear singlemode fibers with a tailored dispersion profile," Opt. Express **19**, 66–80 (2011).
[241]C. Baskiotis, A. Heidt, S. Alam, and D. Richardson, "LMA effectively single-mode thulium doped fibre with normal dispersion at wavelengths around 2 μm," in *Conference on Lasers & Electro-Optics Europe* (IEEE, 2013), pp. CJ–10–4.
[242]S. S. Aleshkina, T. A. Kochergina, V. V. Velmiskin, K. K. Bobkov, M. M. Bubnov, M. V. Yashkov, D. S. Lipatov, M. Yu Salganskii, A. N. Guryanov, and

M. E. Likhachev, "High-order mode suppression in double-clad optical fibers by adding absorbing inclusions," Sci. Rep. **10**, 7174 (2020).
[243]S. V. Firstov, S. V. Alyshev, K. E. Riumkin, V. F. Khopin, A. N. Guryanov, M. A. Melkumov, and E. M. Dianov, "A 23-dB bismuth-doped optical fiber amplifier for a 1700-nm band," Sci. Rep. **6**, 28939 (2016).
[244]D. Darwich, R. Dauliat, R. Jamier, A. Benoit, J.-L. Auguste, S. Grimm, J. Kobelke, A. Schwuchow, K. Schuster, and P. Roy, "50.4% slope efficiency thulium-doped large-mode-area fiber laser fabricated by powder technology," Opt. Lett. **41**, 384–387 (2016).
[245]R. Gumenyuk, E. O. Okhotnikova, V. Filippov, D. A. Korobko, I. O. Zolotovskii, and M. Guina, "Fiber lasers of Prof. Okhotnikov: Review of the main achievements and breakthrough technologies," IEEE J. Sel. Top. Quantum Electron. **24**, 1–14 (2017).
[246]S. Hochheim, E. Brockmüller, P. Wessels, M. Steinke, J. Koponen, T. Lowder, S. Novotny, J. Neumann, and D. Kracht, "Integrated fiber components based on chirally-coupled-core fibers for all-fiber amplifier," in *Fiber Lasers and Glass Photonics: Materials through Applications II* (International Society for Optics and Photonics, 2020), Vol. 11357, p. 113570Y.
[247]M. Pawliszewska, A. Dużyńska, M. Zdrojek, and J. Sotor, "Wavelength-and dispersion-tunable ultrafast holmium-doped fiber laser with dual-color operation," Opt. Lett. **45**, 956–959 (2020).
[248]L. G. Holmen, P. C. Shardlow, P. Barua, J. K. Sahu, N. Simakov, A. Hemming, and W. A. Clarkson, "Tunable holmium-doped fiber laser with multiwatt operation from 2025 nm to 2200 nm," Opt. Lett. **44**, 4131–4134 (2019).
[249]X. Cheng, Z. Li, J. Hou, and Z. Liu, "Gain-switched monolithic fiber laser with ultra-wide tuning range at 2 μm," Opt. Express **24**, 29126–29137 (2016).
[250]H. Ahmad, A. Sharbirin, A. Muhamad, M. Samion, and M. Ismail, "2 μm mode-locked thulium-doped fiber laser using Mach–Zehnder interferometer tuning capability," Laser Phys. **27**, 065104 (2017).
[251]G. Yang, Y.-G. Liu, Z. Wang, J. Lou, Z. Wang, and Z. Liu, "Broadband wavelength tunable mode-locked thulium-doped fiber laser operating in the 2 μm region by using a graphene saturable absorber on microfiber," Laser Phys. Lett. **13**, 065105 (2016).
[252]N. Li, M. Liu, X. Gao, L. Zhang, Z. Jia, Y. Feng, Y. Ohishi, G. Qin, and W. Qin, "All-fiber widely tunable mode-locked thulium-doped laser using a curvature multimode interference filter," Laser Phys. Lett. **13**, 075103 (2016).
[253]V. Kamynin, S. Kablukov, K. Raspopin, S. Antipov, A. Kurkov, O. Medvedkov, and A. Marakulin, "All-fiber Ho-doped laser tunable in the range of 2.045−2.1 μm," Laser Phys. Lett. **9**, 893 (2012).
[254]Q. Fang, K. Kieu, and N. Peyghambarian, "An all-fiber 2-μm wavelength-tunable mode-locked laser," IEEE Photonics Technol. Lett. **22**, 1656–1658 (2010).
[255]T. Tiess, A. Hartung, M. Becker, M. Rothhardt, R. Dauliat, B. Leconte, G. Humbert, P. Roy, and M. L. Jäger, "Tunable fiber laser concepts in the 2-μm spectral range for tunable dual wavelength emission (conference presentation),ŠŠ in *Fiber Lasers and Glass Photonics: Materials through Applications II* (International Society for Optics and Photonics, 2020), Vol. 11357, p. 1135714.
[256]E. Hernández-Escobar, M. Bello-Jiménez, A. Camarillo-Avilés, R. López-Estopier, O. Pottiez, M. Hernández-Arriaga, M. Durán-Sánchez, B. Ibarra-Escamilla, and M. Andrés, "Broadband tuning of a long-cavity all-fiber mode-locked thulium-doped fiber laser using an acousto-optic bandpass filter," Opt. Lett. **44**, 4183–4186 (2019).
[257]J. Kim and Y. Song, "Ultralow-noise mode-locked fiber lasers and frequency combs: Principles, status, and applications," Adv. Opt. Photonics **8**, 465–540 (2016).
[258]X. Li, K. Wu, Z. Sun, B. Meng, Y. Wang, Y. Wang, X. Yu, X. Yu, Y. Zhang, P. P. Shum *et al.*, "Single-wall carbon nanotubes and graphene oxide-based saturable absorbers for low phase noise mode-locked fiber lasers," Sci. Rep. **6**, 25266 (2016).
[259]K. Wu, J. H. Wong, Z. Luo, C. Ouyang, P. Shum, and Z. Shen, "Phase noise and timing jitter eliminator for mode-locked lasers based on external graphene layers," in *Optical Fiber Communication Conference* (Optical Society of America, 2011), p. OThL5.
[260]A. S. Mayer, W. Grosinger, J. Fellinger, G. Winkler, L. W. Perner, S. Droste, S. H. Salman, C. Li, C. M. Heyl, I. Hartl *et al.*, "Flexible all-PM NALM Yb:fiber laser design for frequency comb applications: Operation regimes and their noise properties," Opt. Express **28**, 18946–18968 (2020).
[261]A. Rampur, Y. Stepanenko, G. Stępniewski, T. Kardaś, D. Dobrakowski, D.-M. Spangenberg, T. Feurer, A. Heidt, and M. Klimczak, "Ultra low-noise coherent supercontinuum amplification and compression below 100 fs in an all-fiber polarization-maintaining thulium fiber amplifier," Opt. Express **27**, 35041–35051 (2019).
[262]H. Cheng, W. Lin, Z. Luo, and Z. Yang, "Passively mode-locked Tm^{3+}-doped fiber laser with Gigahertz fundamental repetition rate," IEEE J. Sel. Top. Quantum Electron. **24**, 1–6 (2017).
[263]C. Mahnke, Y. Ma, S. Salman, C. M. Heyl, and I. Hartl, "A passively mode-locked holmium fiber oscillator based on a nonlinear amplifying loop mirror operating at 2050 nm," in *9th EPS-QEOD Europhoton Conference* (European Physical Society, 2020), Vol. 44A, pp. tu–m2–3.
[264]P. Kadwani, R. A. Sims, J. Chia, F. Altal, L. Shah, and M. C. Richardson, "Atmospheric gas detection using broadband mid-IR thulium fiber-based sources," in *Laser Technology for Defense and Security VII* (International Society for Optics and Photonics, 2011), Vol. 8039, p. 80390L.
[265]I. Mingareev, F. Weirauch, A. Olowinsky, L. Shah, P. Kadwani, and M. Richardson, "Welding of polymers using a 2 μm thulium fiber laser," Opt. Laser Technol. **44**, 2095–2099 (2012).
[266]S. Mishra and V. Yadava, "Laser beam micromachining (LBMM)—A review," Opt. Lasers Eng. **73**, 89–122 (2015).
[267]N. Gehlich, T. Bonhoff, L. Sisken, M. Ramme, C. Gaida, M. Gebhardt, I. Mingareev, L. Shah, and M. C. Richardson, "Utilizing the transparency of semiconductors via 'backside' machining with a nanosecond 2 μm Tm:fiber laser," in *Laser-Based Micro-and Nanoprocessing VIII* (International Society for Optics and Photonics, 2014), Vol. 8968, p. 89680W.
[268]B. Voisiat, D. Gaponov, P. Gečys, L. Lavoute, M. Silva, A. Hideur, N. Ducros, and G. Račiukaitis, "Material processing with ultra-short pulse lasers working in 2 μm wavelength range," in *Laser Applications in Microelectronic and Optoelectronic Manufacturing* (International Society for Optics and Photonics, 2015), Vol. 9350, p. 935014.
[269]M. C. Pierce, S. D. Jackson, P. S. Golding, B. Dickinson, M. R. Dickinson, T. A. King, and P. Sloan, "Development and application of fiber lasers for medical applications," in *Optical Fibers and Sensors for Medical Applications* (International Society for Optics and Photonics, 2001), Vol. 4253, pp. 144–154.
[270]N. G. Horton and C. Xu, "Dispersion compensation in three-photon fluorescence microscopy at 1700 nm," Biomed. Opt. Express **6**, 1392–1397 (2015).
[271]Y. Nomura, H. Murakoshi, and T. Fuji, "Short-wavelength, ultrafast thulium-doped fiber laser system for three-photon microscopy," OSA Continuum **3**, 1428–1435 (2020).
[272]J. P. Marangos, "High-harmonic generation: Solid progress," Nat. Phys. **7**, 97–98 (2011).
[273]G. Scurria, I. Manek-Hönninger, J. Carré, A. Hildenbrand-Dhollande, and S. Bigotta, "7 W mid-infrared supercontinuum generation up to 4.7 μm in an indium-fluoride optical fiber pumped by a high-peak power thulium-doped fiber single-oscillator," Opt. Express **28**, 7672–7677 (2020).
[274]D. Jain, R. Sidharthan, G. Woyessa, P. M. Moselund, P. Bowen, S. Yoo, and O. Bang, "Scaling power, bandwidth, and efficiency of mid-infrared supercontinuum source based on a GeO_2-doped silica fiber," J. Opt. Soc. Am. B **36**, A86–A92 (2019).